AD623128

AD

USAAVLABS TECHNICAL REPORT 65-60

DYNAMIC ELASTIC, DAMPING, AND FATIGUE CHARACTERISTICS OF FIBERGLASS-REINFORCED SANDWICH STRUCTURE

By

Gene M. Nordby
W. C. Crisman
Charles W. Bert

CLEARINGHOUSE FOR FEDERAL SCIENTIFIC AND TECHNICAL INFORMATION

Hardcopy	Microfiche		
$3.00	$0.75	94 pp.	as

ARCHIVE COPY

October 1965

U. S. ARMY AVIATION MATERIEL LABORATORIES
FORT EUSTIS, VIRGINIA

CONTRACT DA 44-177-AMC-164(T)
UNIVERSITY OF OKLAHOMA RESEARCH INSTITUTE

[illegible]

BLANK PAGES
IN THIS
DOCUMENT
WERE NOT
FILMED

DEPARTMENT OF THE ARMY
U. S ARM AVIATION MATERIEL LABORATORIES
FORT EUSTIS, VIRGINIA 23604

This research effort was carried out under Contract DA-44-177-AMC-164(T) by the University of Oklahoma Research Institute.

The report has been reviewed by the US Army Aviation Materiel Laboratories and is considered to be technically sound.

The conclusions made by the contractor are considered by this Command to be valid.

TASK 1P121401A14176
CONTRACT DA 44-177-AMC-164(T)
USAAVLABS Technical Report 65-60
October 1965

DYNAMIC ELASTIC, DAMPING, AND FATIGUE CHARACTERISTICS OF FIBERGLASS-REINFORCED SANDWICH STRUCTURE

Final Report

by
Gene M. Nordby
W. C. Crisman
Charles W. Bert

Prepared by
University of Oklahoma Research Institute
Norman, Oklahoma

For
U. S. ARMY AVIATION MATERIEL LABORATORIES
FORT EUSTIS, VIRGINIA

ABSTRACT

Research was conducted to determine the basic dynamic properties of fiberglass-reinforced plastic (FRP) sandwich structure suitable for use as a primary airframe structural material. The research program was carried out in two separate parts: (A) determining dynamic moduli and damping, and (B) determining fatigue behavior. In each part, two types of hexagonal-cell honeycomb core materials were investigated: 5052 aluminum foil and HRP (heat resistant phenolic) fiberglass. The selection of the sandwich configuration and fabrication procedures was based upon previous research carried out at the University of Oklahoma Research Institute for USAAVLABS (USATRECOM TR 64-37 and USAAVLABS TR 65-66).

PREFACE

This report was prepared by the University of Oklahoma Research Institute under Phase II of U. S. Army Transportation Research Command (USATRECOM) Contract DA 44-177-AMC-164(T). Phase I, which pertains to fabrication is reported separately. The research effort is a continuation of the work done in two other USATRECOM contracts which resulted in the following reports: Research in the Field of Fiberglass-Reinforced Sandwich Structure for Airframe Use and Strength Properties and Relationships Associated With Various Types of Fiberglass Reinforced Facing Sandwich Structure. The present report contains the test results, conclusions, and recommendations for research conducted on dynamic properties of fiberglass-reinforced sandwich structure, including dynamic elastic moduli, damping characteristics, and flexural fatigue properties, during the period of April 9, 1964, to November 30, 1964.

This report was written by Dr. Gene M. Nordby, project director and Dean of the College of Engineering at the University of Oklahoma; Mr. W. C. Crisman, project engineer; and Dr. Charles W. Bert, research engineer and Associate Professor of Aerospace and Mechanical Engineering. Mr. Donald Hanson worked as test engineer and statistician.

CONTENTS

ILLUSTRATIONS

TABLES

SYMBOLS

a	amplitude
A	shear area (i.e., cross-sectional area of core)
b	bending flexibility parameter ($\equiv \omega L^2 \sqrt{M/EI}$)
B	beam cross-sectional width
c	core thickness
C_D	material-damping coefficient defined in Equation (40)
$C_1, \ldots, C_4$	constants of integration in expression for Y
$C_1', \ldots, C_4'$	constants of integration in expression for S
D	specific damping energy (i.e., internal energy dissipated per unit volume per cycle)
$d_a/2$	effective centroidal distance of core-to-facing adhesive from centroid of the composite
E	dynamic elastic modulus of facings
$\bar{E}$	complex modulus defined in Equation (42)
E_d	damping modulus
f	natural frequency of composite beam, cps ($\equiv \omega/2\pi$)
g	gravitational constant, 386 in/sec^2
G	dynamic shear modulus of core
h	total depth of beam ($\equiv c + 2\,t_f$)
I	area moment of inertia of the facings about the beam neutral axis
J	composite-beam mass moment of inertia per unit length of beam
K	transverse-shear coefficient (i.e., shape factor)
L	beam length

m	material-damping exponent defined in Equation (40)
M	composite-beam mass per unit length
n	number of cycles
r	rotatory inertia parameter ($\equiv \sqrt{J/A}\,/L$)
s	shear flexibility parameter ($\equiv \sqrt{EI/GAK}\,/L$)
S	normal mode form of ψ
t	time
t_a	effective thickness of core-to-facing adhesive
t_f	thickness of one facing
w_a	specific weight of core-to-facing adhesive, psi
w_c	specific weight of core, psi
w_f	specific weight of one facing, psi
x	position along the beam length
x_N	position of a node
y	total lateral deflection
Y	normal mode shape (i.e., normal mode form of y)
α	dimensionless parameter defined by Equation (A-14)
β	dimensionless parameter defined by Equation (A-15)
γ	$(\cosh b\alpha - \cos b\beta) / (\lambda \sinh b\alpha - \zeta \sin b\beta)$
δ	logarithmic decrement
ϵ	position parameter ($\equiv x/L$)
ϵ_N	node position parameter ($\equiv x_N/L$)
ζ	$(\beta^2 - s^2) / (\alpha^2 + s^2)$
λ	α/β
ρ	effective density of composite ($\equiv M/Bc$)

σ	stress amplitude
ψ	slope of beam deflection due to flexure only
ω	natural frequency of composite beam, radians/sec
ω_s	natural frequency for pure shear vibration according to three-dimensional elasticity theory
ω_s'	natural frequency for pure thickness-shear vibration according to Timoshenko beam theory

SUMMARY

The research covered in this report consists of the determination of the basic dynamic properties of fiberglass-reinforced plastic (FRP) sandwich structure suitable for use as a primary airframe structural material. The research program was carried out in two separate parts: (A) determining dynamic moduli and damping, and (B) determining fatigue behavior. In each part, two types of hexagonal-cell honeycomb core materials were investigated: 5052 aluminum foil and HRP (heat resistant phenolic) fiberglass. The selection of the sandwich configuration and fabrication procedures was based upon previous research carried out at the University of Oklahoma Research Institute for USAAVLABS (references 29 and 30).

In the dynamic moduli and damping experiment, beam strips were suspended at the nodes for the lowest symmetrical mode and excited acoustically at the frequency corresponding to this mode. Then the power was cut off and the decay in facing strain at the beam center line was recorded versus time. By means of a new refined vibration analysis of sandwich beams, it was possible to use the static moduli (the modulus of elasticity of the facings and the shear modulus of the core) to predict the lowest natural frequency and corresponding node location. Over the frequency range covered (300 to 700 cps), the agreement between predicted and measured values was good, so that it was concluded that the dynamic moduli were the same as the corresponding static moduli. The damping was determined directly in terms of the logarithmic decrement for free vibration of the composite. The log decrement values obtained ranged from 0.023 to 0.049, with the values for the fiberglass-core beams generally slightly higher than those for the aluminum-core beams. There was no significant effect of stress level on damping (up to the maximum stress level covered, 1270 psi), but there was an effect of frequency, the peak occurring at approximately 500 cps.

In the fatigue experiment, a special specimen and an associated loading fixture were devised to subject a test length of the specimen to a cyclic constant bending moment along the test length. Exitation was provided by an electromagnetic exciter with force control achieved by use of a piezoelectric force gage. No significant difference was found between the fatigue behavior of the specimens with aluminum cores and those with fiberglass cores. There was no apparent endurance limit within 10 million cycles of load as often occurs in metals. However, design for various cyclic lives can be accomplished in terms of corresponding fatigue strength values. Thus, the life corresponding to a stress amplitude of 38 per cent of the ultimate static strength is approximately 10^5 cycles, while for a stress of 29 per cent, the life is approximately 10^7 cycles.

DISCUSSION

PART A - DYNAMIC MODULI AND DAMPING

1. Introduction

The objective of the dynamic moduli and damping phase of the research was to obtain experimentally the two properties for fiberglass-reinforced plastic (FRP) sandwich suitable for use in primary aircraft structure. The dynamic moduli sought were the dynamic modulus of elasticity of the facings and the dynamic shear modulus of the core. Logarithmic decrement (defined in section A4a) was selected as the measure of damping.

In particular, the sandwich construction evaluated consisted of fiberglass-epoxy facings and honeycomb cores of either aluminum or HRP fiberglass. Prior to the present work, very little information had been obtained regarding the dynamic properties of this very promising structural material. As discussed in the literature reviews that follow, apparently there are no tests directly comparable to those reported here.

In these tests recently conducted at the University of Oklahoma Research Institute (OURI), the dynamic properties were determined at five first-mode frequencies ranging from 300 to 700 cps, and, in addition, the logarithmic decrement was determined at five facing stress-amplitude levels ranging from 270 to 1270 psi at each frequency. A new, refined vibration analysis for sandwich-type beams was developed to facilitate the calculation of the dynamic moduli from the precise frequency and node measurements made in the laboratory. The logarithmic decrement was determined by measurement of the decay of free vibrations with time. A significant aspect of the program is that all of the required data for a given type sandwich construction and a given frequency were measured on a single beam specimen.

2. Description of Experiment

The experiment consisted of taking measurements on a series of beam strips sized in length to resonate as closely as possible to the following frequencies: 300, 400, 500, 600, and 700 cps. While suspended in the free-free condition, the exact frequencies and flexural node locations were recorded for sinusoidal exitation by acoustical means. Then the exitation was cut off and photographs were taken of the decaying facing-strain oscillations. The details of the work are presented on the following pages.

a. Test Specimens

The structural sandwich tested consisted of fiberglass-epoxy facing laminates separately bonded to hexagonal-cell honeycomb

cores. The laminates were fabricated in the following manner using E-glass, 181-weave, fiberglass fabric and EPON 828 epoxy resin activated by curing agent Z.

The fabric was impregnated with heated resin in a multi-ply coating machine designed and constructed for USAAVLABS in a previous program (reference 30) and modified as a part of Phase I of the present contract (reference 29). Three layers of fabric were simultaneously impregnated by the vat and roller system to form a pre-preg which was allowed to partially cure (B-stage) for 10 hours at room temperature. The material was then cut to facing size (22 x 28 inches for the aluminum-core panels or 19 x 28 inches for the fiberglass-core panels) and placed in cold storage until used.

The facing cure was accomplished in a hydraulic press equipped with electrically heated platens. The pre-preg was thawed, the thin polyethylene protective films were removed, and the raw laminate was placed between thin caul sheets using 6-mil polyvinyl alcohol (PVA) film for a parting agent. The caul sheets and laminate were placed in the press set at 160 degrees Fahrenheit, precured without pressure for 8 minutes, and then cured for the remainder of 90 minutes under 30-psi pressure. In Phase I of this research program (reference 29), these conditions of cure were observed to produce a good balance between surface smoothness and strength properties. After cure in the press, the laminates were then post-cured in a recirculating, hot-air oven for 2 hours at 300 degrees Fahrenheit.

One facing laminate was taken from the sandwich program, cut into specimens, and tested for strength properties. The details of specimen preparation and test precedure are discussed in reference 29. The test data are presented in Table 1 on the following page. The average thickness of the facings was 0.0339 inch at an average resin content of 35.7 per cent. It was noted that these laminates possessed excellent surface smoothness, but were slightly lower in ultimate strength than those previously produced by OURI (reference 30). These conditions are attributed to the shorter pre-cure phase employed in the cure cycle--only 50 per cent of the resin gel time.

Two core materials manufactured by Hexcel Products, Inc. were used in this study of dynamic properties of sandwich. These were 3/4-inch-thick, 3/16-inch hexagonal cell honeycomb constructed of (1) 5052 aluminum, 1-mil perforated foil (density = 3.1 pounds per cubic foot) and (2) fiberglass (HRP-heat resistant phenolic, density = 4.4 pounds per cubic foot). The shear properties of these cores were determined by test according to paragraph 5.1.5 of reference 38. The data are tabulated in Table 1.

TABLE 1
PROPERTIES OF SANDWICH CONSTITUENTS

Constituent	Thickness* (in.)	Specific Weight* (psi)	Number Specimens	Load Orient.+	Type Loading	Strength* (psi)	Number Specimens	Modulus* (psi)	Number Specimens
Facing** (resin content: 35.7%)	0.0418 0.0339 0.0245	1.980×10^{-3} 1.950×10^{-3} 1.900×10^{-3}	12	(=W)	Tension	45,100 37,300 29,100	15	3.99×10^{6} 2.95×10^{6} 2.43×10^{6}	14
				(=W)	Compress.	44,900 40,500 30,400	13	4.34×10^{6} 3.72×10^{6} 3.11×10^{6}	11
Aluminum Core (5052-0.001P, 3/16-inch cell)	3/4 (nominal)	1.372×10^{-3} 1.345×10^{-3} 1.323×10^{-3}	5	(=R)	Shear	233 200 216	35	47,000 40,700 34,200	35
HRP Core (GF-11, 3/16-inch cell)	3/4 (nominal)	1.991×10^{-3} 1.890×10^{-3} 1.815×10^{-3}	7	(+R)	Shear	200 181 154	27	7,000 6,200 5,220	27
Adhesive*** (AF-110B)	0.010 (nominal)	5.556×10^{-5}	-	-	-	-	-	-	-

* Values Listed Vertically in the Order of High, Average, and Low.

** The facing properties were obtained from one laminate only, except in the case of the specific weight measurements where the sampling represents 12 laminates.

*** Data From Minnesota Mining and Manufacturing Company "Technical Data Sheet, Issue Number 1," Dated October, 1961.

+ The symbols = and + are used to indicate whether the load was oriented parallel or perpendicular, respectively, to the fabric warp direction (W) or the core ribbon direction (R).

The sandwich assembly was accomplished in the press at 350 degrees Fahrenheit under 10-psi pressure for 40 minutes. Minnesota Mining and Manufacturing Company's film-supported adhesive, AF-110B, was used to effect the core-to-facing bond. For the aluminum core, the ribbon was oriented parallel to the facing fabric warp direction; for the HRP-fiberglass core, the ribbon was oriented perpendicular to the warp direction. This was necessary in the latter case because the HRP core could be purchased only with a 19-inch dimension in the ribbon direction.

Prior to sandwich assembly, precise determinations were made of the core and facing specific weights. These values are also presented in Table 1. The specimens weighed for these determinations were all of sandwich panel size.

After fabrication, the sandwich panels were cut into 3-inch-wide strips with their length directions parallel to the facing fabric warp direction and earmarked for either the damping or the fatigue program by use of a random number table. The strips assigned to the damping program were further trimmed to length on a table saw equipped with an abrasive-wheel blade, the exact lengths of the beam strips being dictated by the test frequency (see the test procedure for the details of cutting). The dimensions of the specimens were measured with the following accuracy: length--within 1/64 inch; width--within 0.01 inch; thickness--within 0.001 inch. On the average, the specimens were 3.0 inches wide and 0.815 inch thick. The remaining data are tabulated in Tables 2 and 3 on pages 12 and 13.

b. Test Apparatus

The apparatus which was used to measure the material damping properties of the FRP facing-honeycomb core structural sandwich consists of an acoustical driving system and a system to detect and record the damped facing strain oscillations of a beam strip specimen. Photographs of the test set-up and the test equipment are presented in Figure 1 and 2, respectively. A block diagram of the entire system is given in Figure 3, along with a list and brief description of the major components of the electronic equipment.

The test apparatus is in essence a vertical, rectangular frame with three plywood cross members (Figure 1). The vertical members of the frame are steel all-thread screws which permit accurate location of the cross members. The two lower cross members support the speakers between which the beam specimen is suspended. The upper cross member supports the specimen by way of nylon lines (0.014-inch diameter) looped around suspension pins pushed into the core in the center of the sandwich thickness dimension and at the flexural nodes. In this configuration the dual speaker system acoustically drives the specimen at its mid-span in free-free flexural vibration.

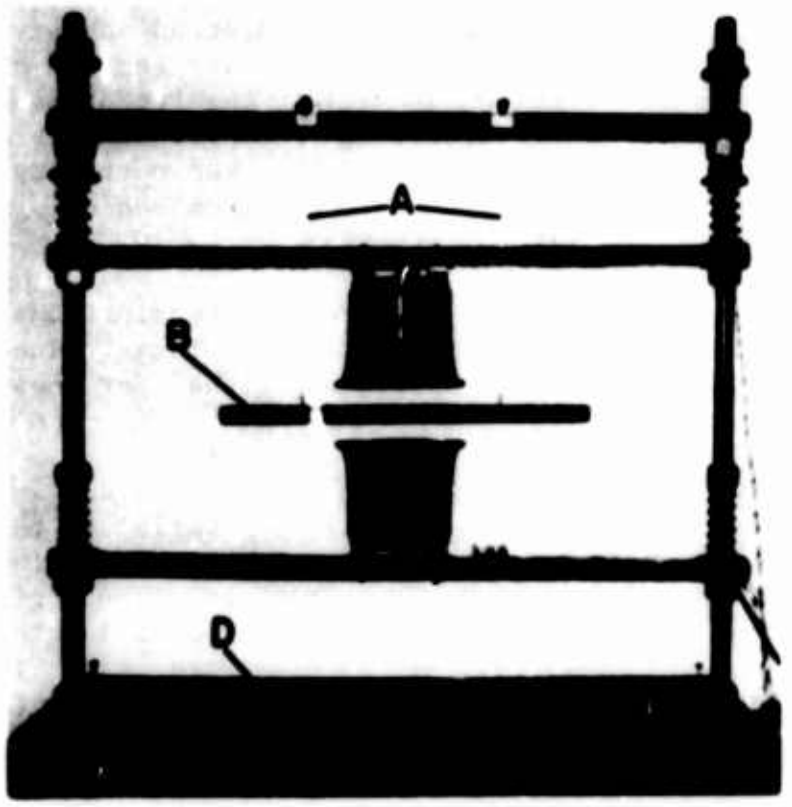

Figure 1. Test Apparatus for Measurement of Dynamic Properties. A, Suspension Lines; B, Test Specimen; C, Driving Speakers; D, Test Stand; E, Trigger Switch.

Figure 2. Electronic Equipment Employed in Measurement of Dynamic Properties. A, Audio Oscillator; B, Frequency Counter; C, Power Amplifier; F, Oscilloscope; G, Oscilloscope Camera and Camera Mount; H, Carrier Amplifier; I, Power Supply; J, Bridge Circuit; K, Carrier Oscillator; L, Battery for Trigger Circuit.

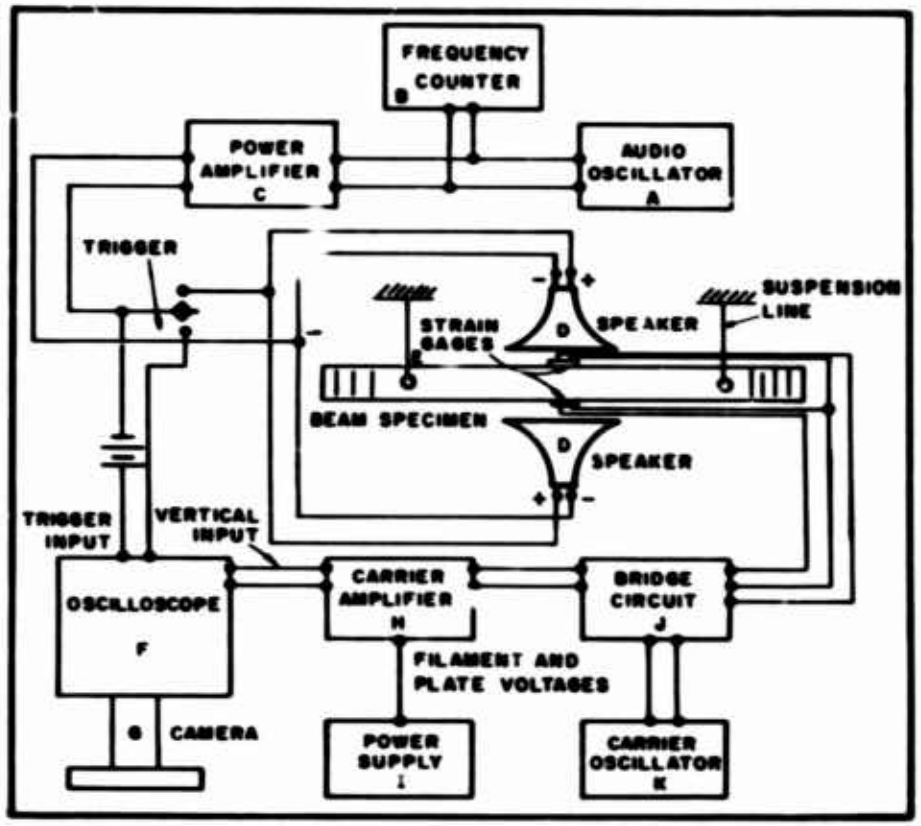

ELECTRONIC EQUIPMENT

(A) Audio Oscillator: The Jackson Electrical Instrument Company Model 652 (frequency range: 20-20,000 cps)

(B) Frequency Counter: Hewlett-Packard Company Model 521G (reads in cps)

(C) Power Amplifier: Sherwood Electronics Laboratories, Inc. Model 1000 (rated: 35 watts; 20-20,000 cps)

(D) Speakers: University Loudspeakers (Division of Ling-Temco-Vought, Inc.) Model ES-50 (rated: 50 watts program material, 250-10,000 cps)

(E) Strain Gages: The Budd Company Metal Film C6-141-B

(F) Oscilloscope: Tektronix, Inc. Model 503

(G) Camera and Mount: Tektronix, Inc. Model C-12

(H) Carrier Amplifier: Two-Stage Triode Amplifier Designed at University of Oklahoma

(I) Power Supply: Lambda Electronics Corporation Model 71

(J) Bridge Circuit: Conventional Full-Wave Bridge with Series Balance

(K) Carrier Oscillator: General Radio Company Type 1203-A (20-500,000 cps)

Figure 3. Wiring Diagram and Instrumentation Used in the Measurement of Dynamic Properties of FRP Facing-Honeycomb Core Sandwich.

The following factors were considered in the choice of the driving speakers: size, power handling capacity, and frequency response. The size of the specimen (3 inches wide) dictated a small speaker to insure maximum concentration of acoustical energy on the specimen. A horn-type (siren) speaker was selected rather than a cone-type because of greater power handling capacity and acoustical efficiency. The energy transfer to the specimen was optimized, not only by using the dual arrangement (speakers operating 180 degrees out of phase), but also by placing an insert (plug) in each horn, which was of optimum depth and diameter of opening (diameter equal to specimen width, see Figure 4). Ideally, the frequency response of the speakers should be flat over the operating range, but in view of the time and cost necessary to develop such a speaker, those commercially available were favored. The particular speaker chosen had the maximum frequency response in approximately the middle of the operating spectrum (300 to 700 cps).

The response of the specimen was detected by strain gages located on the top and bottom facings at the mid-span. The recording system included an AC bridge circuit, an AC amplifier, and an oscilloscope with camera attachment. The AC bridge was selected in order to use the reliable, low-cost AC amplifier. The particular amplifier used was chosen for its low noise characteristics. A carrier frequency of 6,000 cps was determined to be optimum for this particular assemblage of equipment. The strain gages were placed in adjacent arms of the bridge relative to the impressed voltage (reference 12) for a larger output signal and for temperature compensation.

The bridge circuit was operated in the unbalanced condition and the signal was not demodulated for the following reasons: (1) all the desired information was displayed in the modulated signal, (2) the signal is usually damaged by the demodulation circuitry, and (3) calibration and photograph measurement are simplified (see data reduction procedure).

The Tektronix 503 oscilloscope with camera attachment (Model C-12) was used to photograph the decaying modulated carrier signal. A two-pole, double-throw switch in a simple battery circuit, as shown in Figure 3, was used to simultaneously interrupt the driving circuit and trigger the oscilloscope.

c. Experimental Procedure

The sandwich strips were first cut to length according to the desired natural frequencies. This was accomplished by trimming the length of the beams by small increments until their lowest natural frequencies approached the desired values. The frequencies were determined with the aid of powdered molybdenum disulphide.

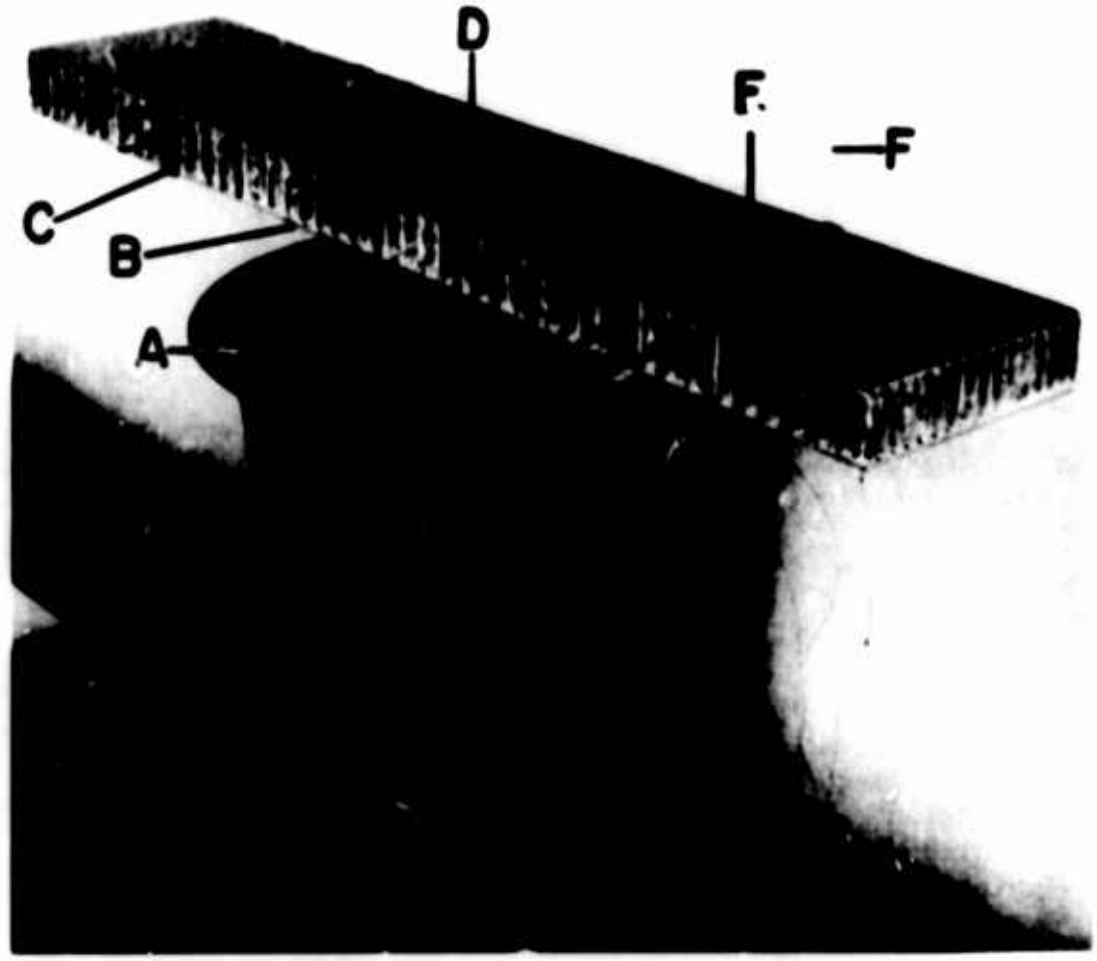

Figure 4. Detail View of Test Set-Up for Measurement of Dynamic Properties. A, Lower Driving Speaker Showing the Insert with the 3-Inch-Diameter Opening (Upper Speaker Has Been Removed); B, Aluminum Core Test Specimen; C, Small Sliding Clip Used in Locating Flexural Nodes; D, Strain Gage; E, Strain Gage Leads; F, Suspension Lines.

The beam strips were suspended in a simple cradle or loop in the vicinity of the node points, and a small amount of the black powder was dusted on the upper facing. The driving frequency was then adjusted until the lowest frequency was found that would cause the powder to collect into a thin line at the node locations.

After the specimens had been tuned (the lengths established), the strain gages were bonded to the top and bottom facings. Eastmen 910 cement was used for this purpose. The gages were located within 1/64 inch of the center of the facings and within 3 degrees of true alignment.

Number 37 copper wire was used for the strain-gage leads. The wires were taped to the facings from the strain-gage connection to the vicinity of the vibration nodes, with small fatigue loops being provided at the gage connections. The lead wires were brought from the specimens at the nodes to minimize energy losses (see Figure 4).

Next, the precise locations of the vibration nodes were determined. For these and the remaining test special effort was made to insure that the driving speakers were vertical and that the specimens were suspended horizontally and in the center of the speaker arrangement.

The specimens were suspended at four points by nylon lines looped around the pins of the small clips shown in Figure 4. Observing the peak-out of the strain-gage signal displayed on the oscilloscope, the previous determination of the specimen natural frequency was confirmed and the exact value was recorded to the nearest cycle per second. With the specimen being driven at this frequency, the black powder was dusted on the upper facing and the suspencion clips were moved along the edge of the specimen until the node lines became straight and the suspension points were located at the ends of these lines. It should be mentioned that the clips were made from 10-mil-thick brass shim stock and, hence, were very light, yet stiff enough to maintain any preset position.

The apparatus was then shut down, and the powder lines were replaced with pencil lines. After the pencil lines had been drawn, three measurements were made of their locations from the ends of the specimens. The average values are recorded in Tables 2 and 3 on pages 12 and 13, respectively.

Although the clips were convenient for the node determinations, aluminum pins pushed into the core midway between the facings was favored as the means of suspension during the damping tests. It was possible to insert the pens within 1/32 inch of the nodes.

With the pins in place, each specimen was again installed in the test apparatus. Both before and after each damping test, polaroid photos were taken of the carrier signal and the carrier signal modified by the shunting of a calibration resistor across an active strain gage. Each specimen was then vibrated at maximum amplitude. The oscilloscope was placed on external trigger and the camera shutter opened in preparation for the photographing of the decaying strain-gage signal. The throwing of the trigger switch followed by the closing of the camera shutter then completed the operation. The film used for these recordings was the Polaroid 3,000 speed, Type 47.

Initially, in the preliminary tests, the speakers were placed as close to the specimens as 1/4 inch to induce the greatest possible facing stresses. However, it appeared that the proximity of the speakers was contributing to the damping of the specimens, and for this reason, a distance of 1 inch was used during the test program. The distance of 1 inch for speaker-specimen separation was determined in an extensive side investigation in which separation distances up to 1.5 inches were compared. The 1-inch distance was the minumum distance at which no speaker damping effects were noted.

The photographs were measured by projecting them onto a large screen where an engineering tape graduated in sixteenths could be used. The average magnification was 12 to 1. The orthogonality of the projection was assured by comparing the magnifications of two accurately measured blocks that had been taped to the left and right sides of the oscilloscope screen and, thus, were photographed with the wave forms. Each carrier and modified carrier signal was measured six times, and the average value in each case was used in the calculations. Only one measurement was made of the peak magnitude of each strain oscillation. Figure 8, on page 35, is a typical photo of the decaying strain signal.

The experimental data are presented in Tables 2 and 3, on the following pages. The calculation procedures and the interpretation of the results are presented in later sections.

3. Dynamic Moduli

Before presenting the new analysis used in this project to determine the dynamic moduli, it is worthwhile to discuss previous analyses of sandwich-beam vibration; this is done in section a that follows. Furthermore, since the new analysis is an extension of the so-called Timoshenko beam theory and since many analyses based on this theory

TABLE 2
LOGARITHMIC DECREMENT AND NODE LOCATIONS,
ALUMINUM HONEYCOMB CORE SANDWICH

Specimen Data*		Logarithmic Decrement at Stress Levels						Node Locations (in.) From	
Length (in.)	Frequency (cps)	270 psi	400 psi	533 psi	670 psi	1,000 psi	1,270 psi	End A	End B
22.88	307	0.0234	0.0247	-	-	-	-	5.26	5.23
19.84	399	0.0355	0.0348	0.0336	0.0326	0.0294	-	4.50**	4.60
17.58	498	0.0391	0.0367	0.0378	0.0388	0.0416	0.0423	4.04	3.99
16.14	600	0.0341	0.0329	0.0372	0.0362	0.0326	0.0356	3.66**	3.75
14.91	705	0.0287	0.0285	0.0316	0.0367	-	-	3.36**	3.43

* The average values of width and thickness for all the specimens were 3.0 inches and 0.815 inch, respectively.

** The double asterisk is used to mark the thickest end of the specimens where the difference is greater than 0.005 inch.

TABLE 3
LOGARITHMIC DECREMENT AND NODE LOCATIONS,
FIBERGLASS HONEYCOMB CORE SANDWICH

Specimen Data*		Logarithmic Decrement at Stress Levels					Node Locations (in.) From	
Length (in.)	Frequency (cps)	270 psi	400 psi	670 psi	1,000 psi	1,270 psi	End A	End B
21.89	302	0.0302	0.0271	-	-	-	5.11	5.02**
18.74	401	0.0351	0.0389	0.0305	0.0310	-	4.39	4.31**
16.62	501	0.0492	0.0454	0.0434	0.0486	0.0427	3.90	3.81**
15.02	603	0.0405	0.0402	0.0391	0.0365	-	3.45	3.51
13.69	706	0.0339	0.0334	0.0339	-	-	3.13**	3.22

* The average values of width and thickness for all the specimens were 3.0 inches and 0.815 inch, respectively.

** The double asterisk is used to mark the thickest end of the specimens where the difference is greater than 0.005 inch.

equation for the natural frequency corresponding to any mode. The primary objection to their analysis, as well as all subsequent energy analyses in this area, is that they computed the energies based on a mode shape assumed to be the same as that of a simple, homogeneous (Bernoulli-Euler) beam. They should have adjusted the mode shape to obtain a minimum value of the natural frequency. Due to the considerable effects of transverse shear and rotatory inertia in a sandwich beam, the adjusted mode shape would be expected to be quite different than the shape they assumed. Thus, the frequency value predicted by their theory would be expected to be higher than the exact value. In their paper, Kimel, Raville, et al published experimental results only for the natural frequencies associated with the fifth and higher modes. Agreement between natural frequencies calculated by using static moduli and the natural frequencies measured experimentally was fair. Theoretical values were high in two tests and low in the other two.

The next paper, by Raville et al (reference 33), also was an energy analysis. The assumptions made were similar to those of Kimel, Raville, et al, except that here the facings were assumed to be identical and the boundary conditions were those for a beam clamped at each end. This analysis did not result in an explicit expression for natural frequency; instead it resulted in a frequency equation in the form of a series requiring 36 terms for proper convergence. In all the beams tested, the theoretical frequency values based on static moduli were higher than the experimentally measured values, as would be expected when an energy method is used and the mode shape is not adjusted as previously described.

The next analysis was one by Glaser (reference 13), in which the rotatory inertia was neglected. There was no good reason to neglect this, since it would have resulted in merely a change in the coefficient of the shear flexibility term in the final differential equation. The natural frequencies of the first five modes were measured for sandwich and monolithic beams with various end conditions. In all cases, the calculated frequency values were much higher than the experimental ones for the first mode, quite close for the second and third modes, and lower than the experimental ones for the fourth and fifth modes. Since this trend was observed even in the case of the monolithic beam, it must be concluded that there was a serious error in either the calculations or the measurements.

In 1961, James (reference 16) made an energy analysis which was very similar to that of Kimel, Raville, et al except that James considered a free-free beam with identical facings. He considered only the lowest natural frequency and obtained an explicit equation for it. Although James obtained good agreement between his

theoretical and experimental values, the theoretical values were higher in eleven out of twelve tests. It should be mentioned that good agreement in terms of natural frequency alone is not sufficient, since node locations may still be in considerable error. Unfortunately, James did not measure the experimental node locations.

The first direct application of Timoshenko beam vibration theory to sandwich beams was made by Clary and Leadbetter (reference 8) in 1963. However, they used the same boundary conditions used by Kruszewski (reference 24) in 1949, which were later shown by others to be incorrect, as discussed in detail in the next section.

The most recent analysis is one by Dar (reference 10), who used an approach similar to that of Raville et al and included the effect of thickness-normal deformation, which turned out to be negligible in practical cases.

b. Literature Review: Timoshenko Beam Theory

The elementary Bernoulli-Euler theory for the vibration of a macroscopically homogeneous beam considers only flexural flexibility and lateral translational inertia. A beam incorporating in addition the effects of transverse-shear flexibility and rotatory inertia is usually referred to as a Timoshenko beam, since the first derivation of the differential equations which govern the motion of such beams is generally attributed to Timoshenko (reference 40). The incorporation of the effect of rotatory inertia alone is generally attributed to Rayleigh (reference 34) in the 1870's, while Timoshenko added the effect of shear flexibility in 1921. However, according to Mindlin and Deresiewicz (reference 27), Bresse (reference 6) as early as 1859 was the first to add both rotatory-inertia and shear-flexibility effects to the simple Bernoulli-Euler beam theory.

Although the so-called Timoshenko beam equations date back many, many years, apparently the most exact boundary conditions for use with them were not derived until 1951, by Dengler and Goland (reference 11), in treating beam impact. The first use of these boundary conditions in beam vibration analysis is due to Anderson (reference 2).

The series solution of Anderson is cumbersome to apply. However, Traill-Nash and Collar (reference 44) obtained a general closed-form solution of the differential equations and gave the resulting frequency equations for a variety of simple boundary conditions (all combinations of fixed, simply supported, and free ends). Recently, Huang (reference 15), apparently unaware of the work of Traill-Nash and Collar, presented an equivalent analysis and also gave equations for the normal mode shapes.

The proper determination of the transverse shear coefficient K for even a beam of homogeneous, isotropic material has also been the subject of considerable controversy. In his original analysis, Timoshenko (reference 40) used the static value of 2/3 for a rectangular section. In a later paper (reference 41), Timoshenko used a static value of 0.889, which was based upon some photoelastic measurements by Filon. In the latest edition of his vibration book (reference 42, page 335), Timoshenko recommends the use of 0.833 for K, which coincides with the results of Reissner's static analysis (reference 35) using a variational principle. As early as 1951, Mindlin (reference 26 and 27) noted that a static value of K is not appropriate, since the problem is a dynamic one. For a homogeneous, isotropic beam of rectangular cross section, he obtained a value of 0.822 for K.

Since the values of 0.833 and 0.822 are very close, there is no significant difference between the static and dynamic values of K for a homogeneous, isotropic beam.

c. New Analysis

In previous work (reference 8) in which the Timoshenko-beam approach was applied to sandwich beams, no mention was made of the value used for the shear coefficient (shape factor) K. Apparently a value in the vicinity of 0.8, which is applicable only to rectangular-cross-section beams of homogeneous construction, was used.

In his energy solution for the vibration of a sandwich beam, James (reference 16) used an effective value of K given by

$$K = 1 + (t_f/c) \qquad (1)$$

where t_f is the thickness of one facing and c is the core thickness. For the sandwich construction with which the present project is concerned, this amounts to a value of 1.04 for K.

The approach used here to arrive at the correct dynamic value of K for a sandwich beam is simply the same approach used by Mindlin (reference 26 and 27) to determine the dynamic value of K for a rectangular-cross-section, monolithic beam.

Application of Equation (A-1) in the Appendix to pure thickness-shear motion requires that y and its derivatives in Equation (A-1) be set equal to zero. Thus, Equation (A-1) reduces to simply

$$\partial\psi/\partial x = 0. \qquad (2)$$

Now putting y = 0 (no bending deflection) and Equation (2) into Equation (A-2) in the Appendix results in the following differential equation in the shear slope:

$$\frac{\partial^2 \psi}{\partial t^2} + \frac{GAK}{J}\psi = 0. \tag{3}$$

From Equation (3), the natural frequency ω'_s (rad/sec) of pure thickness-shear vibration according to the Timoshenko-beam theory is

$$\omega'_s = (GAK/J)^{1/2}. \tag{4}$$

However, according to the three-dimensional theory of elasticity, the natural frequency ω_s for a rectangular cross-sectional element (of the core) of depth c in pure shear motion is (reference 43)

$$\omega_s = (\pi/c)\ (G/\rho)^{1/2} \tag{5}$$

where ρ is the effective density. Using total mass of the facings and core gives

$$\rho = M/Bc \tag{6}$$

where B is the beam cross-sectional width.

Equating ω'_s in Equation (4) to ω_s in Equation (5), incorporating Equation (6), and simplifying:

$$K = (J/M)\ (\pi/c)^2. \tag{7}$$

It is to be noted that Equation (7) shows that for a sandwich beam of rectangular cross section, K depends upon the combination of rotatory mass moment of inertia, mass, and core depth. This is in contrast to a monolithic beam of rectangular cross section, for which K is equal to $\pi^2/12$ (≈0.822) regardless of the beam mass or cross-sectional dimensions. However, as a check of Equation (7), if the specific relationship for J/M which holds for a monolithic rectangular cross section, namely,

$$J/M = 1/3\ (c/2)^2 = c^2/12,$$

is substituted into Equation (7), the result is $K = \pi^2/12$, which checks.

The considerable difference between the shear coefficient of a sandwich beam and that of a monolithic beam is shown in the next section, which covers a sample calculation.

In a previous research investigation (reference 22), measured natural frequency has been used in conjunction with theoretical analysis to calculate the dynamic shear modulus G of the core, assuming that the dynamic elastic modulus E of the facing is equal to the measured value of the static elastic modulus. However, this violates the basic principles of good experimentation, since there is no more basis for assuming that E has a dynamic value equal to its static value than for making the same assumption for G.

In another study (reference 13), experimental results obtained for one set of boundary conditions were used to determine the dynamic value of G, and then this value of G was used to compute the natural frequencies associated with other sets of boundary conditions. These latter values were then compared with the measured natural frequencies for the other conditions to assess the accuracy of the frequency analysis. The agreements between theory and experiment were poor perhaps because of two reasons: (a) the theory was too crude, and (b) different boundary conditions results in different natural frequencies and yet both E and G may be frequency dependent. One way to overcome this difficulty would be to use beams of different lengths with the different boundary conditions and to select these lengths so that there would always be at least one pair of sets of boundary conditions for each frequency. However, this approach still requires a large number of beams with at least two different kinds of support conditions.

In order to reduce the number of tests and the number of kinds of support fixtures required in the present project, it was desired to arrive at a method of obtaining sufficient information from a vibration test of a given beam specimen vibrating at one frequency (the lowest natural frequency) to be able to determine the dynamic values of both E and G at that frequency. The method devised to achieve this objective is the simple one of measuring the node location in addition to the lowest natural frequency. (Node locations are determined quite easily experimentally by sprinkling fine powder on the specimen. The location to which the powder moves is the node location. This was the method used many years ago to obtain the famous "Chadnai figures" associated with plates vibrating in various modes.)

To establish the validity of the concept used, it must be shown that:

(1) The theoretical expressions for natural frequency and node location depend upon E and G.

(2) For a beam of given geometry and composed of core and facing materials of given density, there is only one

unique combination of values for E and G which will result in the measured combination of lowest natural frequency and the associated node locations.

To meet the first requirement mentioned, it is noted that from the second of Equations (A-8) in the Appendix, the natural frequency depends upon E and the parameter b^2. To calculate the node locations, the right-hand side of Equation (A-26) in the Appendix must be set equal to zero to obtain the following equation:

$$\cosh b\alpha\epsilon - \lambda\gamma \sinh b\alpha\epsilon + (1/\zeta) \cos b\beta\epsilon - \gamma \sin b\beta\epsilon = 0. \qquad (8)$$

The value of ϵ which satisfies Equation (8) is the dimensionless position at which the node occurs, denoted by ϵ_N ($\epsilon x_N/L$, where x_N is the actual position of the node). From Equation (8), ϵ_N depends upon the parameter b. Thus, both the natural frequency and the node location depend upon the value of b. From the frequency equation, Equation (A-24) in the Appendix, the value of b depends upon the value of s^2, which in turn depends upon the ratio E/G, as is easily seen from the definition of s^2 in the last of Equations (A-8) in the Appendix. Thus, it has been shown that ω depends upon both E and E/G and that γ depends upon only E/G.

From the foregoing, it is seen that although a given node location x_N does not uniquely determine a single combination of values of E and G, it does establish the necessary condition that whatever be the values of E and G, they must have a certain ratio E/G. Establishment of the E/G ratio establishes a unique value for s^2, which for a given mode in turn establishes a unique value for b^2 by virtue of Equation (A-24) in the Appendix, and thus, from the definition of b^2 in the second of Equations (A-8) in the Appendix, establishes a unique value of E. Now there can be only one unique set of values of E and G which meets the requirements of a unique value of E and a certain ratio E/G.

d. Sample Calculation

All of the calculations were carried out using the following average properties and dimensions:

Beam Width: B = 3.00 inches

Facing:

Effective modulus (average of tension and compression values): $E = 3.33 \times 10^6$ psi

Specific weight per facing: $\omega_f = 0.00195$ lb/in^2

Thickness per facing: $t_f = 0.0339$ inch

Core:		**Aluminum**	**Fiberglass**
Shear Modulus:	$G =$	40,700 psi	6,200 psi
Specific weight:	$w_c =$	0.001345 psi	0.00189 psi
Thickness:	$c =$	0.747 inch	0.747 inch

Adhesive:

Shear modulus: included in the measurement of core shear modulus.

Specific weight per layer: $w_a = 0.000556$ psi

Effective thickness per layer: $t_a = 0.010$ inch

Twice the effective centroidal distance from centroid of composite: $d_a = 0.737$ inch

Using the above values, the various parameters required in the analysis were first calculated. An aluminum-core beam is used to illustrate the procedure.

$$M = (2w_f + 2w_a + w_c)\,(B/g) = (2 \times 0.00195 + 2 \times 0.000556 + 0.001345)\,(3/386)$$

or

$$M = 4.94 \times 10^{-5} \text{ lb-sec}^2/\text{in}^2$$

$$A = Bc = 3.00 \times 0.747 = 2.24 \text{ in}^2$$

$$I = \frac{Bt_f\,(c + t_f)^2}{2} + \frac{Bt_f^3}{6} \approx 1/2\,(3.00)\,(0.0339)\,(0.781)^2 = 0.0306 \text{ in}^4$$

$$J = \frac{B}{12g}\left[\frac{w_f}{t_f}h^3 + \left(\frac{w_c}{c} - \frac{w_f}{t_f} + \frac{w_a}{t_a}\right)c^3 - \frac{w_a}{t_a}d_a^3\right]$$

$$= \frac{3}{12 \times 386}\left[\frac{0.00195}{0.0339}(0.815)^3 + \left(\frac{0.001345}{0.747} - \frac{0.00195}{0.0339} + \frac{0.000556}{0.010}\right)(0.747)^3 - \frac{0.000556}{0.010}(0.737)^3\right]$$

$$= 5.70 \times 10^{-6} \text{ lb-sec}^2$$

$$K = (J/M)(\pi/c)^2 = (5.70 \times 10^{-6}/4.94 \times 10^{-5})$$

$$(\pi/0.747)^2 = 2.04$$

Then for the aluminum-core beam with a length of 22.88 inches, the dimensionless parameters b^2, r^2, and s^2 are:

$$b^2 = \frac{4\pi^2 ML^4}{EI} f^2 = \frac{4(9.87)(4.94 \times 10^{-5})(22.88)^4}{(3.33 \times 10^6)(0.0309)} f^2 =$$

$$52.0\,(f/100)^2 \qquad (9)$$

$$r^2 = J/ML^2 = 5.70 \times 10^{-6}/\left[(4.94 \times 10^{-5})(22.88)^2\right] =$$

$$2.20 \times 10^{-4}$$

$$s^2 = \frac{EI}{GAKL^2} = \frac{(3.33 \times 10^6)(0.0309)}{(40{,}700)(2.24)(2.04)(22.88)^2} = 10.56 \times 10^{-4}.$$

The transcendental equation to be solved is Equation (A-24) developed in the Appendix. It is repeated here for convenience.

$$2(1 - \cosh b\alpha \cos b\beta) + \frac{b}{(1 - b^2r^2s^2)^{1/2}}\left[b^2r^2(r^2 - s^2)^2 + (3r^2 - s^2)\right] \sinh b\alpha \sin b\beta = 0, \qquad (10)$$

where

$$\alpha = (1/\sqrt{2})\left\{-(r^2 + s^2) + \left[(r^2 - s^2)^2 + (4/b^2)\right]^{1/2}\right\}^{1/2} \qquad (11)$$

$$\beta = (1/\sqrt{2})\left\{(r^2 + s^2) + \left[(r^2 - s^2)^2 + (4/b^2)\right]^{1/2}\right\}^{1/2} \qquad (12)$$

The procedure used to solve the above system of equations is as follows:

(1) Select a trial value of f and calculate a corresponding value of b^2 using Equation (9).

(2) Using this value for b and previously calculated values for r and s, values are calculated for α and β by means of Equations (11) and (12).

(3) The above values of b, r, s, α, and β are used to compute the value of the left-hand side of Equation (10).

(4) The above procedure is repeated until, by iteration, the magnitude of the left-hand side of Equation (10) is as close to zero as possible. The nearest integer value of frequency (cps) to the lowest one which makes the left-hand side of Equation (10) equal to zero is taken as the answer (i.e., the calculated value of the lowest natural frequency).

In the example, the 22.88-inch-length aluminum-core beam, the final value of the lowest natural frequency f was 308 cps. This gave $b^2 = 494$, $\alpha = 0.2106$, and $\beta = 0.2136$.

Having determined the value of the frequency f, the next step in the calculations is the calculation of the node location x_N. The procedure for doing this is as follows:

(1) Assume a value of ϵ and use it to compute the value of the left-hand side of Equation (8), repeated here for convenience:

$$\cosh b\alpha\epsilon - \lambda\gamma \sinh b\alpha\epsilon + (1/\zeta)\cos b\beta\epsilon - \gamma \sin b\beta\epsilon = 0 \quad (8)$$

where

$$\lambda = \alpha/\beta$$

$$\zeta = (\beta^2 - s^2) / (\alpha^2 + s^2)$$

$$\gamma = (\cosh b\alpha - \cos b\beta) / (\lambda \sinh b\alpha - \zeta \sin b\beta)$$

(2) The above procedure is repeated until, by iteration, the magnitude of the left-hand side of Equation (8) is as close to zero as possible. The nearest value of ϵ, to three significant figures, to the one which makes the left-hand side of Equation (8) equal to zero is taken as the dimensionless value ϵ_N corresponding to the node location.

(3) Finally the distance of the node location from the end of the beam is $x_N = L\epsilon_N$.

In the example, $\epsilon_N = 0.225$ and $x_N = 5.15$ inches.

e. Results and Evaluation

The results of the experimental measurements and the calculations of the lowest natural frequency and node location for each beam are summarized in Table 4 and in Figures 5 and 6. It is emphasized that the calculated values are based on static values of the appropriate mechanical properties (facing modulus of elasticity and core shear modulus).

As can be seen in Table 4, the greatest discrepancy between measured and calculated values is only 6.0 per cent. This is quite good in view of the scatter in facing thickness and in total beam thickness from beam to beam, since the calculations were based on mean values of these quantities.

It is interesting to note that all of the methods of calculation of sandwich-beam natural frequencies utilizing an energy approach are based on the assumption that the node locations are the same as for a simple Bernoulli-Euler beam, which has no shear flexibility and no rotatory inertia. This location is 0.22L, which does not compare very favorably with the locations determined experimentally in this project; these ranged from 0.225L to 0.235L.

The experimentally determined location of the node was different at each end of each beam; however, the maximum difference from one end to the other end of the same beam was only 2.9 per cent. This is attributed to small variations in the mass and stiffness properties along the length of the beam (see Tables 2 and 3). For example, there was a variation in total beam thickness of approximately 0.005 inch from one end to the other on the beam which had a 2.9 per cent variation in node location.

In view of the good agreement (within experimental accuracy) between the measured values and those calculated on the basis of the static moduli, it was decided not to go into the iterative procedure described in section A3c for calculating the dynamic moduli. In other words, it was concluded that the dynamic elastic modulus of the fiberglass facings and the dynamic shear moduli of both the aluminum core and the fiberglass core were the same as their respective static values. This is in agreement with previous work by Richter (reference 36) on fiberglass in the form of tubes.

4. Damping

The literature on the internal damping properties of macroscopically homogeneous materials is voluminous. Although previous investigations of vibration damping in sandwich type construction apparently have been limited to a few independent investigations, in each of these a method was developed to predict the damping behavior of the composite, assuming knowledge of the damping properties of each of the component materials.

TABLE 4
COMPARISON OF MEASURED AND CALCULATED VALUES
OF LOWEST NATURAL FREQUENCY AND NODE LOCATION

Core Material	Beam Length (in.)	Lowest Natural Frequency Exp.* (cps)	Calc.** (cps)	% Diff***	Node Location, Measured From End Experimental* (in.) End A	End B	Calc.** (in.)	% Diff*** End A	End B
Aluminum	14.91	705	712	1.0	3.36	3.43	3.34	-0.6	-2.6
	16.14	600	608	1.3	3.66	3.75	3.62	-1.1	-3.5
	17.58	498	517	3.8	4.04	3.99	3.94	-2.5	-1.3
	19.84	399	406	1.8	4.50	4.60	4.47	-0.7	-2.8
	22.88	302	308	2.0	5.26	5.23	5.15	-2.1	-1.5
Fiberglass	13.69	706	748	6.0	3.13	3.22	3.13	0	-2.8
	15.02	603	625	3.7	3.45	3.51	3.43	-0.6	-2.3
	16.62	501	519	3.6	3.90	3.81	3.79	-2.8	-0.5
	18.74	401	416	3.7	4.39	4.31	4.25	-3.2	-1.4
	21.89	302	309	2.3	5.11	5.02	4.95	-3.1	-1.4

* Experimental values were taken from Tables 2 and 3

** Calculated Values Based on Static Values of Facing Modulus of Elasticity and Core Shear Modulus.

*** % Difference = 100 (Calc. - Exp.) / Exp.

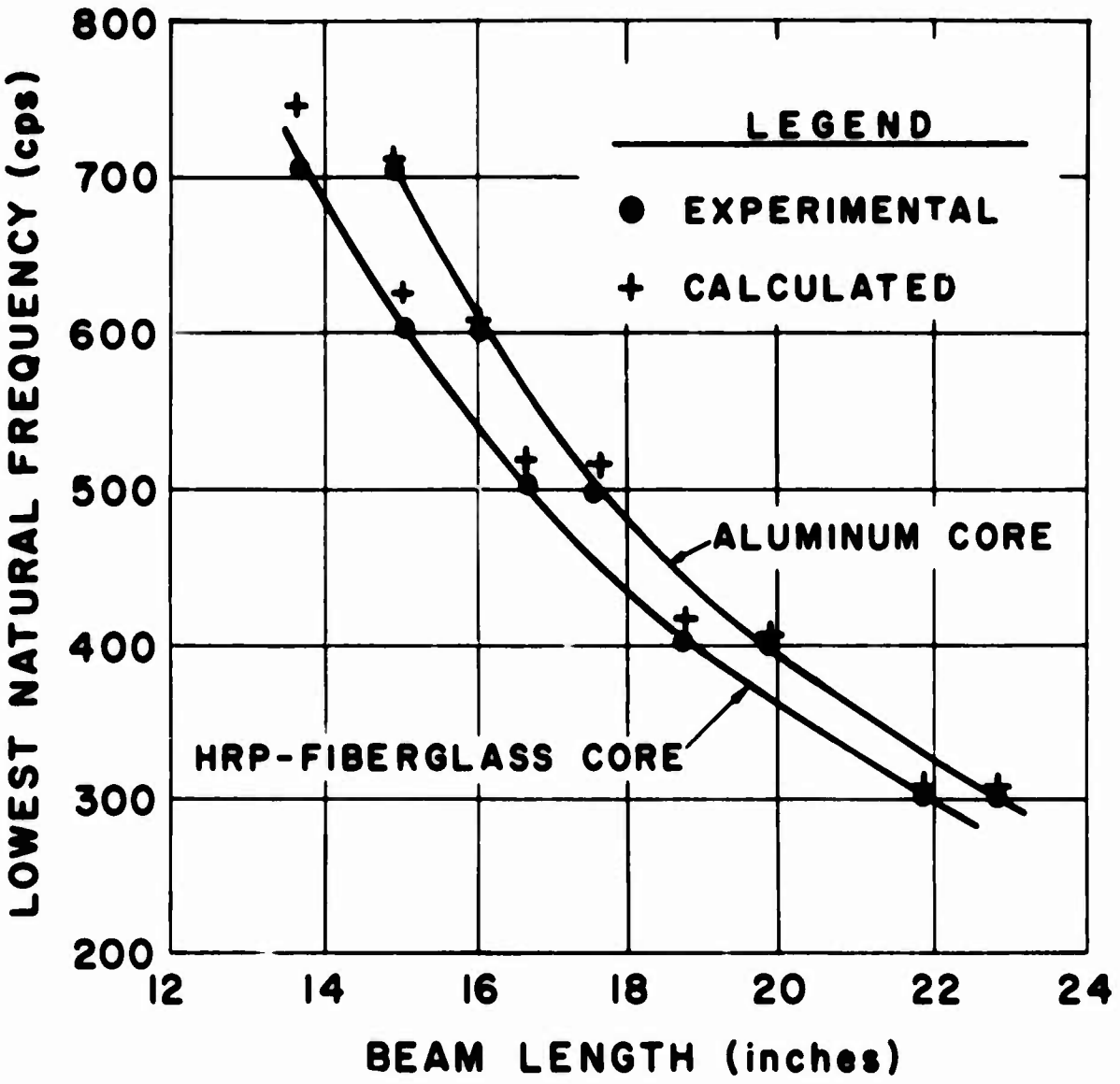

Figure 5. The Effect of Beam Length on Lowest Natural Frequency for Sandwich Beams with FRP Facings and Honeycomb Cores of Aluminum and HRP Fiberglass.

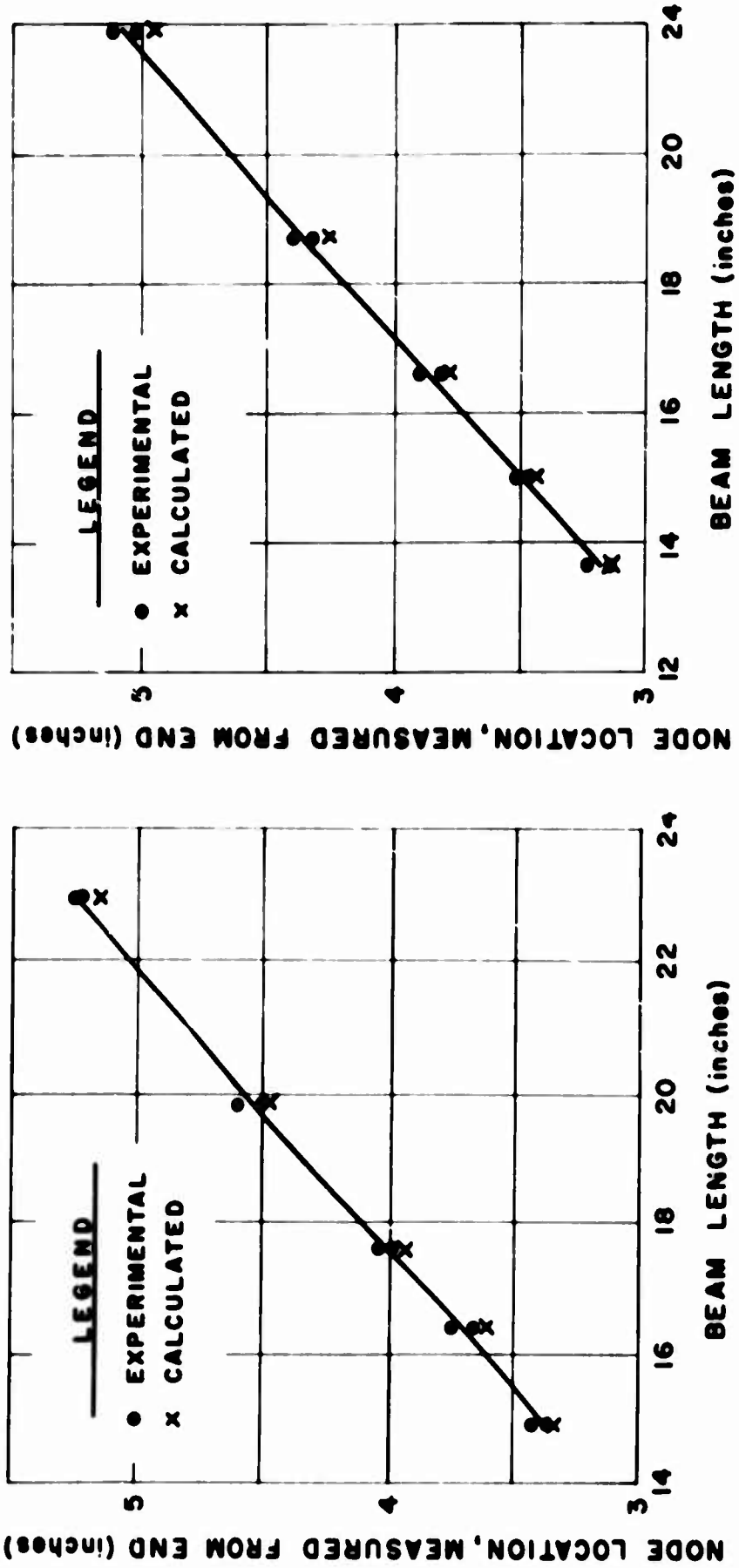

Figure 6. The Effect of Beam Length on Location of Node at Lowest Natural Frequency for Sandwich Beams with FRP Facings and Honeycomb Cores.

Before discussing these previous investigations and their relation to the present study, it is well to describe the various ways of measuring or specifying vibration damping. This is done in the next section.

a. Measures of Vibration Damping

There are four basic ways of measuring or specifying vibration damping (reference 45):

(1) Energy dissipation under steady-state cyclic conditions.

(2) Resonant amplification factor under steady-state cyclic conditions.

(3) Phase lag between stress and strain under steady-state cyclic conditions.

(4) Decay of free vibrations.

Energy dissipation under steady-state conditions is usually determined in terms of energy dissipated per cycle. However, since the energy dissipated per cycle depends upon the size, shape, and stress distribution per cycle, the energy dissipation is usually specified in terms of specific damping energy, which is usually considered to be a more basic material parameter. Specific damping energy is defined as the energy dissipated by damping in a unit volume of material at a given stress level. It is usually specified in units of inch-pound/cubic inch-cycle.

The resonant amplification factor is defined as the ratio of the response to the excitation, with both the response and the exitation specified in terms of the same units. Unfortunately, the resonant amplification factor is dependent upon the system configuration as well as upon the damping property of the material, so that it is not considered to be a basic material property.

The stress-strain lag is usually specified in terms of a phase angle (ωt) in radians. Although this is a dimensionless factor, like the two preceding measures of damping it can be determined directly only by measurements made during steady-state forced vibration. Measurements made under these conditions are likely to be inaccurate due to losses in the excitation equipment.

The decay of free vibrations is usually specified in terms of the logarithmic decrement δ, which is defined as follows:

$$\delta \equiv \ln (a_i/a_{i+1}) \qquad (38)$$

where a_i is the amplitude of a particular quantity (deflection, strain, or stress) in a particular cycle i (see Figure 7) and a_{i+1} is the amplitude of the succeeding cycle. Since the logarithmic decrement of nearly all materials is a very small quantity, it is difficult to measure a_i and a_{i+1} with sufficient accuracy to calculate δ reliably by using Equation (38). Thus, it is customary to assume that δ does not change significantly over a few cycles n (see Figure 7) and to calculate δ from the following equation:

$$\delta = \frac{1}{n} \ln \frac{a_i}{a_{i+n}} . \tag{39}$$

The procedure used for determining damping in this project was to measure the decay of maximum strain level and to apply Equation (39), using strain amplitudes.

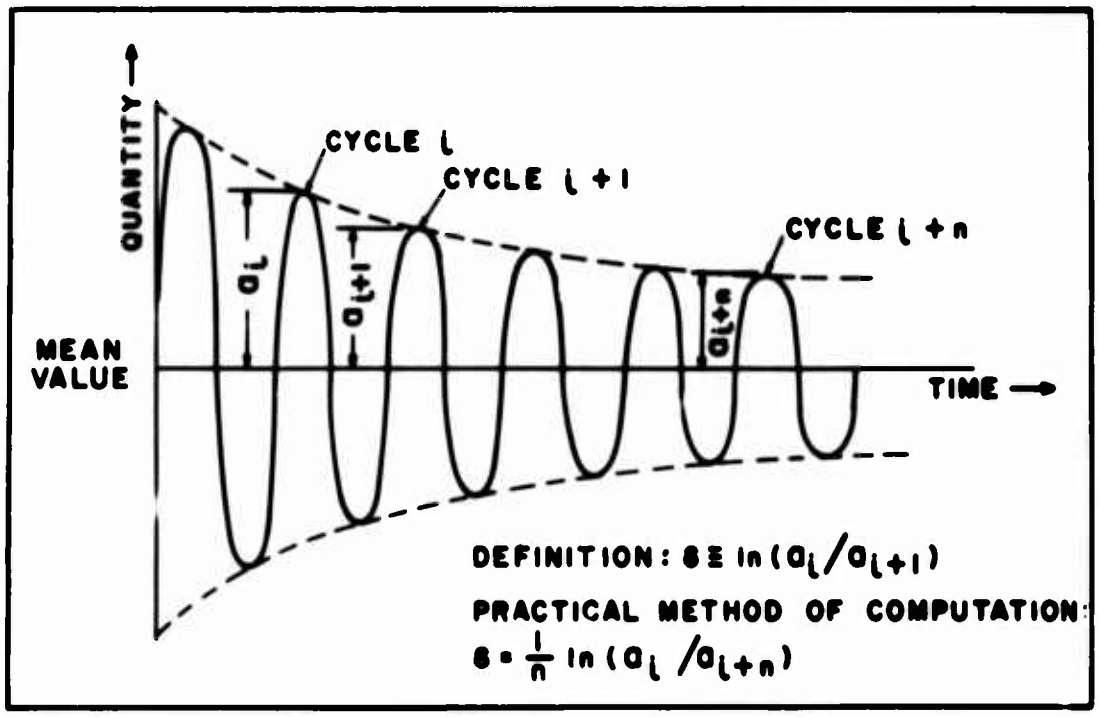

Figure 7. Decay of a Damped Free Vibration Illustrating Quantities Related to Definition and Practical Calculation of the Logarithmic Decrement.

Early experiments by Kimball and Lovell (reference 20) on the damping of a wide variety of materials indicated that the energy dissipation per cycle was proportional to the square of the vibration-displacement amplitude (and thus, also proportional to the square of the stress amplitude). Thus, damping of this nature is often called material damping, hysteretic damping, or structural damping. However, in order to avoid confusion in this report, this type of damping will be referred to as Kimball-Lovell damping. More extensive studies conducted by Lazan (reference 25) have indicated that the specific damping energy D can be more generally represented by the following relation:

$$D = C_D \sigma^m \tag{40}$$

where σ is the stress amplitude and C_D and m are temperature dependent material constants for stress levels up to approximately 80 per cent of the endurance-limit stress under completely reversed stresses.

The specific damping energy D is related to the logarithmic decrement δ by the following approximate relationship:

$$D = \delta \sigma^2 / E \tag{41}$$

where E is the dynamic elastic modulus. Thus, by comparing Equations (40) and (41), it is seen that for a material with Kimball-Lovell damping (m = 2), the logarithmic decrement is independent of stress amplitude. Furthermore, if the exponent m increases with stress to values greater than two (as it does for many metallic materials for stress amplitudes approaching the endurance-limit stress), δ also increases with stress.

A final way of specifying damping properties is in terms of the loss modulus. This concept is applicable only to materials with Kimball-Lovell damping, i.e., m = 2 in Equation (40), since for such a system the sum of the damping force and the spring force (force due to material stiffness) can be represented by a single complex spring constant. In terms of materials properties rather than specific system performance, this implies a single complex modulus $\bar{E}$,

$$\bar{E} = E + iE_d, \tag{42}$$

where E is the dynamic elastic modulus (also known as the storage modulus and the stiffness modulus), $i = \sqrt{-1}$, and the E_d is the damping modulus (also known as the loss modulus). The ratio E_d/E is called the loss factor. Since the loss factor is also equal to the tangent of the phase angle lag between stress and strain, it is sometimes called the loss tangent.

The loss factor is related to the logarithmic decrement by the following approximation:

$$E_d/E \approx \delta/\pi. \tag{43}$$

This relationship permits calculation of the damping modulus from values of the dynamic elastic modulus and the logarithmic decrement, as follows:

$$E_d = E\ \delta/\pi. \tag{44}$$

b. Literature Review: Vibration Damping of Sandwich Structure

Among the earliest analyses of vibration damping of ordinary (three-layer) sandwich structures were the approximate analyses of Plass (reference 31) and of Ross et al (reference 37). These analyses treated sandwich plates, and the approach used was to determine the total effective stiffness of the composite plate and then to replace this stiffness by a complex stiffness.

A more exact analysis of damping in sandwich plates was carried out by Yu (reference 49), using a differential-equation-of-motion approach. His analysis incorporated loss factors associated with flexural motion of the facings and with shear motion of the core; so in effect he assumed that these materials behaved in damping as Kimball-Lovell materials. Unfortunately, Yu's theory is rather complicated to apply and so far as known has never been verified experimentally.

One of the most significant investigations of damping in sandwich construction is the analysis published by Keer and Lazan (reference 19) in 1961. This consisted of both theoretical and experimental studies. The theoretical approach used was to first carry out a vibration analysis of a beam with free ends and central point excitation. From this analysis, they determined the bending-stress distribution in the facings and the shear-stress distribution throughout the core. Then, assuming that both the core and facing materials had Kimball-Lovell damping, the total energy dissipated per cycle was determined by integration over the entire volume of the materials. The core damping properties were obtained experimentally using the procedure previously established by James and Norris (reference 17). Keer and Lazan also made some calculations and carried out some experiments to indicate the relative unimportance of external damping due to aerodynamic friction.

Keer and Lazan measured the total damping (neglecting air friction) for (a) four different beam configurations with 2024-T3 aluminum-alloy facings and aluminum honeycomb cores, (b) one with 2024-T3 facings and a balsa core, (c) another with 2024-T3 facings and a

paper honeycomb core, and (d) another with facings and core of glass-fiber-reinforced plastic. There was very good agreement between theory and experiment for material combinations (a), (b), and (c), above, at maximum stress levels up to 1,000 to 1,200 psi. Above this stress range, the experimentally measured damping values began to increase at a gradually increasing slope, as would be expected in view of the similar behavior of homogeneous 2024 aluminum alloy. Theoretical damping values were not determined for the glass-fiber-reinforced plastic beam (d) due to a lack of sufficient data for the component materials. However, it is curious to note that unlike the other material combinations, this material combination had a constant exponent m of approximately 2.25 over the entire stress range covered.

It is somewhat surprising that such good agreement was obtained by Keer and Lazan between their theoretical and experimental results in view of the many gross approximations which had to be made in their vibration analysis. The largest approximation is the complete neglect of both transverse shear flexibility and rotatory inertia. Thus, the mode shape they used is actually that of a simple Bernoulli-Euler beam.

The next investigation of sandwich-beam vibration damping, which was apparently carried out independently of the work of Keer and Lazan, was that of James (reference 16). His theoretical approach was basically similar to that used by Keer and Lazan, except that James' vibration analysis was considerably more refined than that of Keer and Lazan insofar as frequency is concerned, since James considered both transverse shear flexibility and rotatory inertia, as described previously. However, since James used an energy method based on the same mode shape as the simple Bernoulli-Euler theory, insofar as computation of total damping is concerned, his analysis does not appear to represent much of an improvement over Keer and Lazan's.

The vibration-damping experiments conducted by James are quite different from those of Keer and Lazan. By means of a loudspeaker, he excited the specimen at its lowest natural frequency. The specimen was suspended at its nodes by means of small wires hooked into the core at the neutral axis. The response was measured near one end of the beam by means of a microphone, and the logarithmic decrement was calculated by using Equation (39), above. Apparently the effect of stress on logarithmic decrement δ was not investigated, since only one value of δ was reported for each specimen. All of the material combinations tested had 1/2-inch-thick, 3003-H19 soft-aluminum honeycomb cores with 3/8-inch cells and with the ribbon direction either parallel or perpendicular to the beam axis. Facings included

two different thicknesses of both soft aluminum and 2024-T3 aluminum alloy. For some of these material combinations, two different adhesive-layer thicknesses were tested. The per cent differences between the calculated and measured values of logarithmic decrement ranged from -77 per cent to +134 per cent. This large discrepancy cannot be explained on the basis of the frequency analysis, since the per cent difference for the frequencies ranged from -0.8 per cent to +18.4 per cent. It is interesting to note that in all six specimens in which core ribbon direction was in the axial direction, the theoretical value of δ was lower than the experimental one, while in five of the six specimens with the core ribbon direction oriented transversely the converse was true.

Apparently the first vibration-damping measurements on a full-scale aircraft primary structural component of sandwich-type construction were those made recently by Hackman et al (reference 14). They tested two horizontal stabilizers of conventional aluminum-alloy construction and two of sandwich construction. The sandwich construction consisted of both facings and core("Raypan" triangular fluted type) of glass-fiber-reinforced plastic (GFRP).

In the first bending mode, which occurred in the frequency range of 18-22 cps in all cases, the GFRP stabilizers exhibited lower logarithmic decrements than the aluminum-alloy stabilizers. This was also true for the average values of logarithmic decrement for the second bending mode which occurred at 70-77 cps in the aluminum stabilizers and approximately 57 cps in the GFRP stabilizers. It should also be noted that there was considerably greater difference between the logarithmic-decrement values for the two aluminum stabilizers than between the values for the two GFRP stabilizers. This can be attributed to differences in rivet fit, which in turn affects the amount of slip damping.

At first, the fact that the values were lower for GFRP seems surprising, since it is generally true that nonmetallic materials exhibit more internal damping than metals. However, it is believed that the difference here is again due to the effect of slip damping in the riveted aluminum structure. If the aluminum stabilizer had been of sandwich-type construction (and thus, not riveted), the damping in the aluminum structure would have been considerably lower. Another point is that the frequency ranges involved in these tests were lower than those usually encountered in vibration-damping tests for material evaluation purposes. It may very well be that the effect of frequency on the δ values of

aluminum and GFRP is such that at low frequencies the two δ versus frequency curves cross. However, this cannot be ascertained quantitatively from the results reported by Hackman et al, since they did not run any damping tests on simple coupons and since they varied frequency and mode together (i.e., they did not have a series of specimens in which they could run tests in the same mode yet at various frequencies).

c. Sample Calculation

Equation (39) on page 29 was followed in calculating the values of logarithmic decrement. The sample calculation presented in the subsequent paragraphs will illustrate the procedure employed, starting with the reading of the photographs.

The photographs obtained in the damping tests resemble the one shown in the accompanying figure for the fiberglass specimen excited at 603 cps (Figure 8). After the wave heights were measured as explained in the experimental procedure, the calibration constants were calculated. This was done by dividing the value of the simulated strain (93 μ in./in.) by the difference between the heights of the modified carrier (under 93 μ in./in. strain simulated by a resistor shunting an active strain gage) and the pure carrier.[1] For the test conditions of the photo in Figure 8, the calculation becomes:

$$\frac{93}{24.876 - 20.421} = 20.88.$$

Next, a plot was made of facing strain versus wave number for each photograph. A smooth curve was drawn through the points, and the strain levels were chosen on which to center the log decrement calculations. The curve for the previous photograph is presented in Figure 9.

For convenience, n was taken equal to 10 in Equation (39), and thus the ratios a_i/a_{i+n} were obtained from the peak strains for the 5th wave on either side of the reference strain. Using the 300 μ in./in. strain level (1,000 psi) for the sample

[1] The calibration resistor could either reduce or enlarge the height of the carrier. It is the absolute value of the difference that is sought.

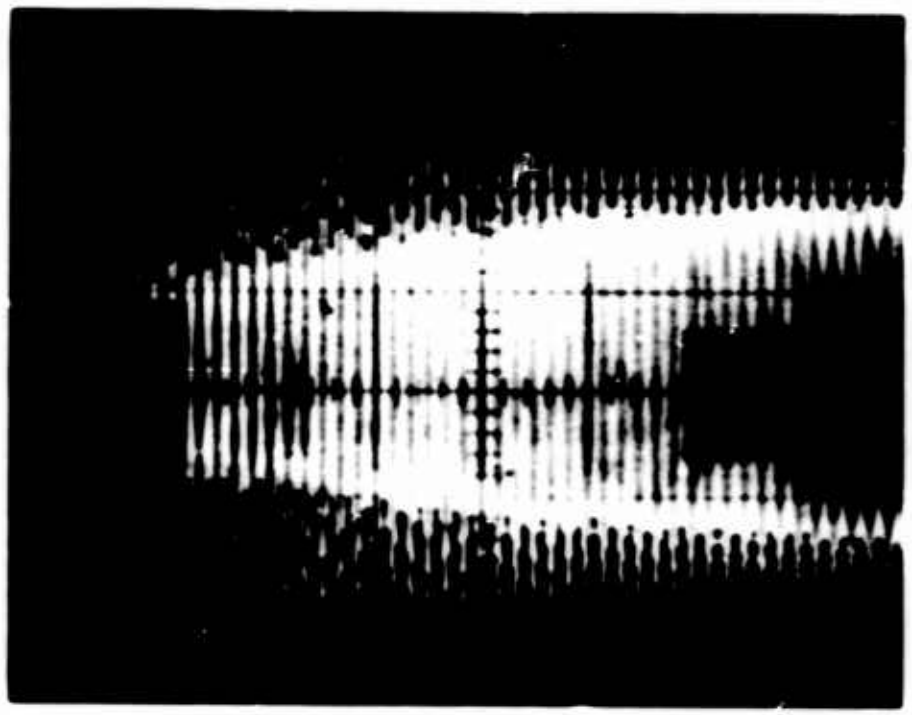

Figure 8. Typical Polariod Photo for Damping Measurements. The decaying strain signal was produced by a fiberglass-core specimen after exitation at its natural frequency of 603 cps.

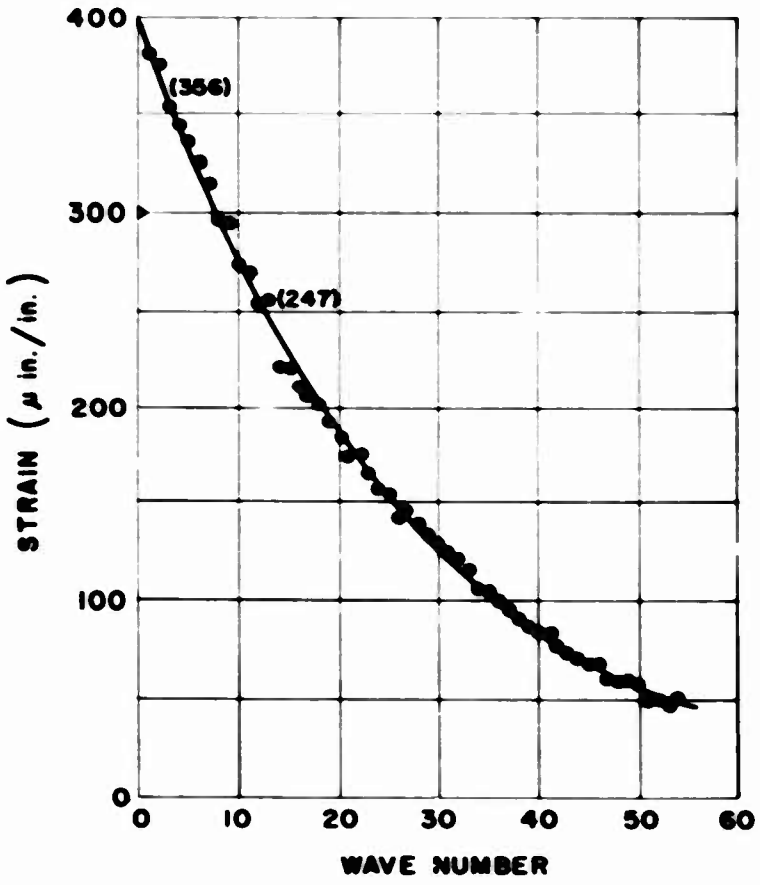

Figure 9. Typical Plot of the Decay of Maximum Facing Strain. These data were obtained from the photo of Figure 8.

calculation, the two values of 356 and 247 μ in./in. were read from the curve in Figure 9 and the log decrement was calculated as follows:

$$\delta = (0.10) \ln (356/247) = (0.10) \ln 1.441$$

$$\delta = 0.0348.$$

d. Results and Evaluation

The measured values of logarithmic decrement are presented in Table 2 for the aluminum-honeycomb-core sandwich and in Table 3 for the fiberglass-honeycomb-core sandwich, on pages 12 and 13, respectively. A comparison of values between these two tables for corresponding conditions (nominal frequency and stress level) indicates the following: In fourteen cases the fiberglass-core sandwich has an appreciably larger log decrement, in two cases the log decrements are approximately the same, and in two cases the aluminum-core sandwich has the larger decrement. From this comparison, it is apparent that, in general, fiberglass-core sandwich material exhibits greater damping than aluminum-core sandwich material.

The effect of frequency on the logarithmic decrement is shown in Figure 10. At first glance, the peak at approximately 500 cps in each case may seem unusual. However, in similar tests on all-aluminum honeycomb beams, James (reference 16) obtained values of log decrement which decreased with increasing frequency from his lowest frequency (459 cps) on up. Whether they would have peaked at 400-500 cps is unknown, since he did not make any measurements below 459 cps. Also, an increasing log decrement versus frequency curve was derived by Richter (reference 36) in the very low frequency range of 0.012 to 1.67 cps for flexural vibration tests of fiberglass tubes. In view of these limited examples, it at least seems plausible that a peak exists in the log decrement versus frequency curve.

The effect of amplitude of stress at the center of the beam, which should be the approximate location of the maximum stress, is shown in Figure 11. Although there is some scatter, there seems to be little effect of stress amplitude on log decrement for a given frequency. This is consistent with core damping data at low amplitudes reported by James (reference 16). As pointed out in section A4a, a log decrement independent of stress amplitude corresponds to a damping energy proportional to the square of the stress amplitude. Thus, the slope of 2.2 for the log-log plot of damping energy versus stress amplitude reported

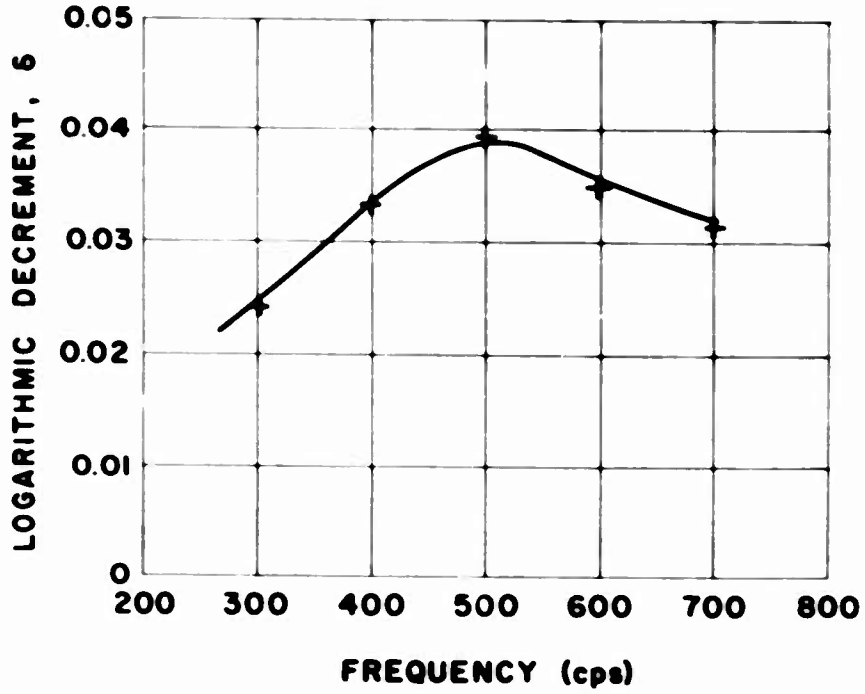

ALUMINUM CORE

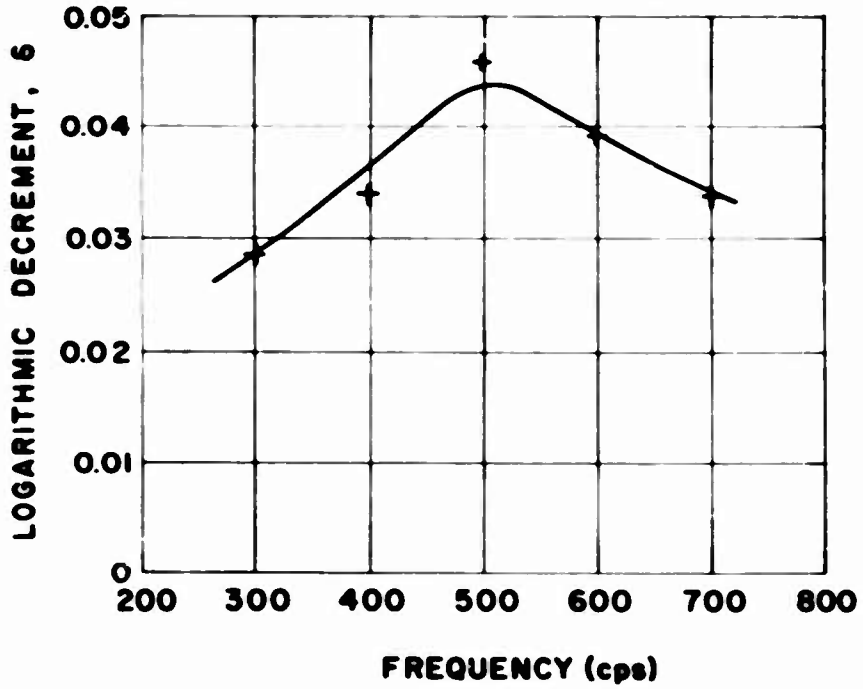

HRP FIBERGLASS CORE

Figure 10. The Relation Between Logarithmic Decrement and Frequency of Vibration for FRP Facing Sandwich Employing Honeycomb Cores. The data points are average values from Tables 2 and 3.

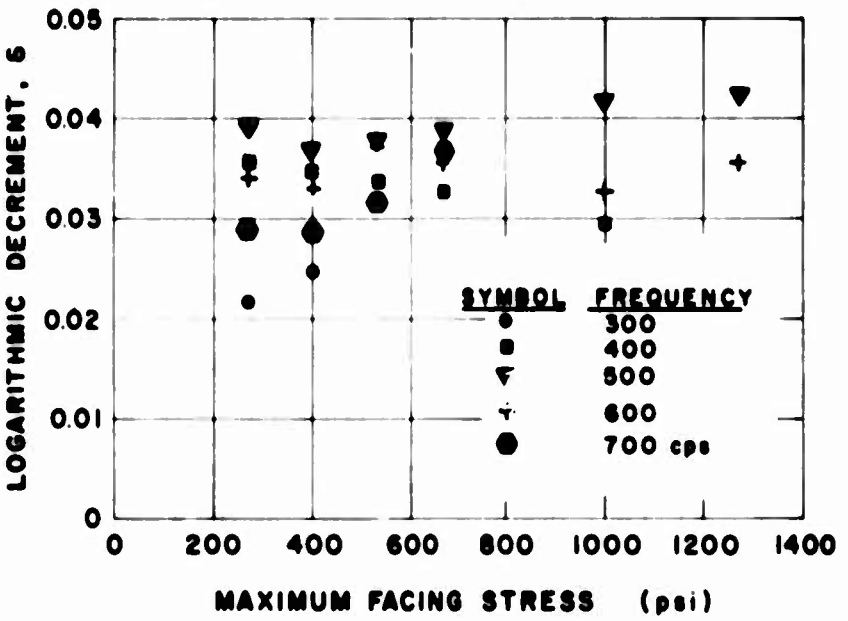

ALUMINUM CORE

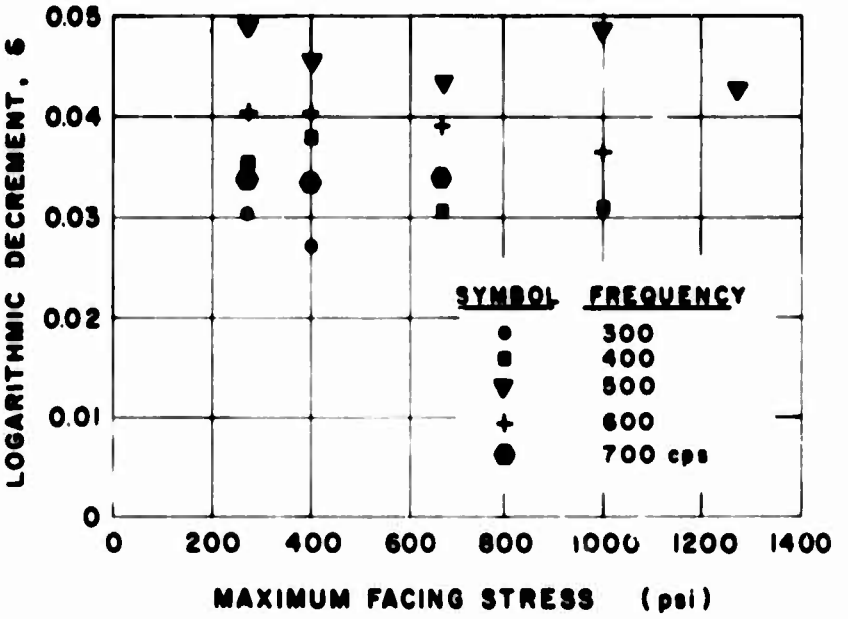

HRP FIBERGLASS CORE

Figure 11. The Variation of Logarithmic Decrement with Maximum Facing Stress at Various Frequencies for FRP Facing Sandwich Employing Honeycomb Cores. The data are from Tables 2 and 3.

by Keer and Lazan (reference 19) for a beam with fiberglass-epoxy facings and fiberglass honeycomb core indicates that they had a log decrement which increased with stress amplitude. Unfortunately it is not possible to convert a damping energy versus stress amplitude plot into a curve of log decrement versus stress amplitude, so that a quantitive comparison cannot be made between Keer and Lazan's results and those reported here.

Although log decrement values cannot be computed for Keer and Lazan's composites, they can be computed for their core shear damping data. Table 5 summarizes logarithmic decrements for the shear-damping tests of Keer and Lazan and of James for various honeycomb-core materials. It is noted that there are few general trends. For example, Keer and Lazan had slightly higher damping for tests in the ribbon direction, while James obtained considerably higher damping for tests perpendicular to the ribbon direction. Nevertheless, all of the values reported in the table fall between 0.0080 and 0.0282, a surprisingly narrow spread. It is expected that the composite would exhibit considerably higher damping than the component materials, as exemplified by the work of James (reference 16). This tends to substantiate the test results obtained in the present project. Further substantiation is shown by the close correspondence between the log decrement values reported here (0.0271 to 0.0486) and those reported by Hackman et al (reference 14) for a horizontal stabilizer of all-fiberglass honeycomb-core sandwich construction (0.033 to 0.048).

TABLE 5
SHEAR DAMPING IN HONEYCOMB-CORE MATERIALS

Honeycomb Core Material	Ribbon Thickness (in.)	Core Thickness (in.)	Cell Shape and Size (in.)	Load Orientation[1]	Logarithmic Decrement (δ)	Data Source (Ref. No.)
Aluminum	0.002	0.500	Hex., 0.25	=R	0.0094	19
Aluminum	0.002	0.500	Hex., 0.25	+R	0.0080	19
Fiberglass	-	0.280	Hex., -	-	0.0098	19
Aluminum	0.001	-	Hex., 0.125	+R	0.0141	16
Aluminum	0.002	-	Hex., 0.375	=R	0.0094	16
Aluminum	0.00-	-	Hex., 0.375	+R	0.0282	16
Aluminum	0.003	-	Hex., 0.375	=R	0.0108	16
Aluminum	0.003	-	Hex., 0.375	+R	0.0160	16

[1] The symbols +R and =R indicate perpendicular and parallel to the ribbon direction, respectively.

5. Conclusions and Recommendations

The major conclusions drawn from the research on dynamic moduli and damping are as follows:

(1) Using the improved analysis presented in this report, it is possible to determine both the facing dynamic modulus of elasticity and the core dynamic shear modulus from measurements of lowest natural frequency and location of the nodes on a single beam.

(2) Using this approach in conjunction with experiments in which the lowest natural frequency and associated node location were measured, it was found that the dynamic moduli were identical to the respective static moduli, within experimental error and over the range of frequencies of 300 to 700 cps and stress levels of 270 to 1,270 psi.

(3) Measurements of the logarithmic decrement for decay of free vibrations gave values ranging from 0.023 to 0.042 for the fiberglass-epoxy facing sandwich with aluminum honeycomb core, and from 0.027 to 0.049 for this type of sandwich with fiberglass honeycomb core. In general, for the same conditions of frequency and facing stress, the fiberglass-honeycomb-core sandwich gave the largest damping values.

In the course of carrying out the research program reported herein, the following logical extensions of the work on dynamic moduli and damping have naturally occurred to the present investigators:

(1) The experiments should be extended to higher vibration modes. For the sake of expediency, the present program was limited to the first mode; however, there is no reason why it could not be extended to higher modes. This would provide additional checks of the analytical methods presented here. Also, it would permit separation of the effects of mode number and frequency per se. This could easily be accomplished by designing one series of specimens so that several selected frequencies would correspond to at least three <u>different modes</u> on different specimens and another series to cover the range of frequencies for a number of selected modes. Cross plotting would permit separation of effects of mode and frequency from frequency per se. It would be expected that mode number would have a major influence on damping since damping is a direct function of the stress distribution which in turn depends upon the modal shape and, thus, the mode number. This would be quite important in connection with designing fiberglass sandwich structures to withstand wideband-frequency excitations.

(2) Experiments should be conducted on beam specimens with lower values of lowest natural frequency. This could be accomplished either by going to free-free beams with a rigid mass attached at each end and the same maximum beam length limitation as encountered here or by using free-free beams without attached masses but of much greater length. The first alternative should permit attainment of a lowest natural frequency near 90 cps. However, this is still high compared to frequencies of interest in many airframe applications. Thus, a combination of the two approaches would probably be required.

(3) A theoretical analysis should be made of the damping in a sandwich beam using specific damping data for the component materials and stress distributions based on the refined modal shapes obtained by the vibration analysis presented in this report. This would be one of the bases for the optimization described below.

(4) Having established a firm basis for the analytical assumptions and having determined the material properties from the sandwich beam work, analyses should be made for vibration of sandwich panels and sandwich shells. (Limited analysis, mostly of an approximate nature, has already been carried out for vibration of rectangular sandwich panels and cylindrical shells.)

(5) In conjunction with the results of the present research in regard to dynamic moduli, damping, and fatigue, as well as the results of items 1 through 4 in this listing, optimum material combinations and sandwich configurations should be determined for various basic structural elements subjected to various types of support and dynamic excitation.

DISCUSSION

PART B - FATIGUE TESTS

1. Introduction

In the fatigue test phase of the investigation there were two objectives: (1) to establish S-N curves for use in designing primary aircraft structural components and (2) to provide a comparison of two types of fiberglass-reinforced sandwich structure, that using the aluminum honeycomb core and that using the HRP fiberglass core.

Since there are many combinations of fiberglass fabric weaves, thickness of laminates for facings, core thicknesses and cell sizes which may be combined with a multitude of combinations of flexure, tension, compression and shear loads, it was impossible to investigate every phase of fatigue. To completely investigate fatigue at this point for sandwich construction would be unwarranted because of the many other factors being investigated, here and elsewhere, which will affect the fatigue characteristics of sandwich construction. Thus, this program was aimed at finding preliminary information which would affect the choice of materials to help optimize other strength and fabrication characteristics in the total program.

It was, therefore, decided to investigate pure flexure loading only. The only tests somewhat similar to these reported here were performed by Keer and Lazan (reference 19), who reported four specimens of a comparable type. The results showed that the fiberglass facing-fiberglass core combination sandwich construction was inferior to aluminum facing-aluminum core and aluminum facing-balsa core combinations. In addition, Keer and Lazan's specimens were vibrated at resonance, and the specimens were double cantilevers driven from a center point on an electromagnetic shaker. This produced a combination of flexure and shear.

The reader is cautioned not to draw sweeping conclusions from fatigue data now available in the literature because fatigue information is incomplete and rather specialized. For example, there are numerous tests on special applications which indicate the superiority of fiberglass laminates in actual structures. Typical of these is the investigation of rotor blades for helicopter use reported by Kaman Aircraft Corporation (reference 18). They report that for a composite sandwich construction rotor blade, a fatigue strength of three times the comparable production model using wood was obtained. This added fatigue strength was achieved with considerable reduction in total weight of the part. In addition, a multi-ply fiberglass laminate bonded sheath over a wood rotor blade substantially improved its fatigue strength characteristics.

On the other hand, most fatigue research indicates that the fatigue strengths of fiberglass structure expressed as a per cent of the ultimate static strength are substantially less than metals. Typical of this is the report by Bert and Hyler (reference 3), which shows that a glass-filiment-wound, epoxy-resin composite had a fatigue strength at 100,000 cycles of approximately 31 per cent of the ultimate tensile strength as compared to a value of 76 per cent for titanium alloy at the same number of cycles.

The point is that fatigue strengths, especially those expressed by ratios or percentages, are not the only criterion on which a material should be judged. Careful consideration by the designer of fatigue strength-to-ultimate static strength ratios, strength-to-weight ratios, and the economics of fabrication will decide this issue when complete data are available. The reduced notch sensitivity, high strength-to-weight ratio, directional strength versatility, and lower tooling costs give fiberglass an advantage in this comparison in the overall picture. The present project is thus aimed only at filling in one facet of the total required information which will aid the designer in making his decision.

2. Description of Experiment

a. Test Specimens

The test specimens were cut from the panels described in Part A for the dynamic moduli and damping investigation (section A2a, page 2).

In the initial fatigue tests, the specimens were cut 3 inches wide and approximately 15 inches long using an abrasive-blade table saw and then ground to final smoothness. This gave a specimen having 18 cells of core material across its width. The specimen was clamped symmetrically in the fatigue apparatus (described later) with 4 inches of the specimen in the clamps at each end, leaving a 7-inch flexure zone in the center portion of the specimen. In these early tests it was learned that the specimens failed near the clamps because of stress concentrations at the edge of the clamp. In addition, there was crushing and abrasion in the clamp area. On the basis of this preliminary testing, the final specimen was developed. None of the preliminary tests were judged valid and are excluded from the report.

The specimen finally selected for testing is shown in Figure 12. It retained the overall length of 15 inches, but the center of the specimen had a narrow section 2 inches wide with 12 core cells across the width. This narrow throat forced the failure to occur in the center section. In order to prevent crushing in the clamps, the core was cut out of the ends of the specimens for a distance

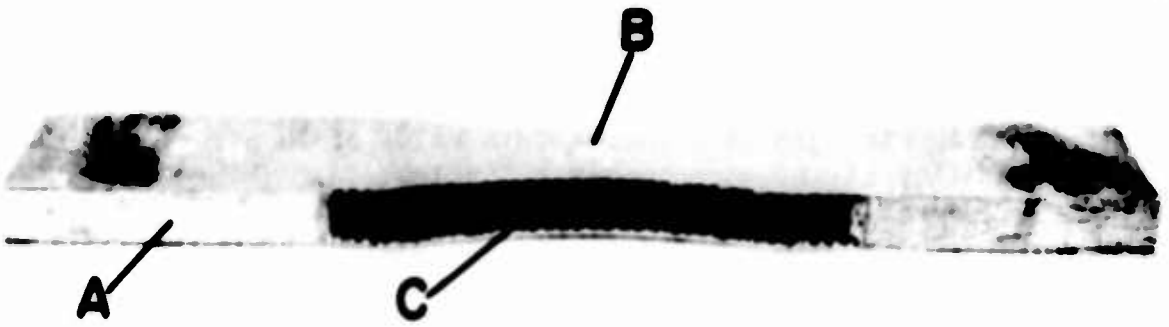

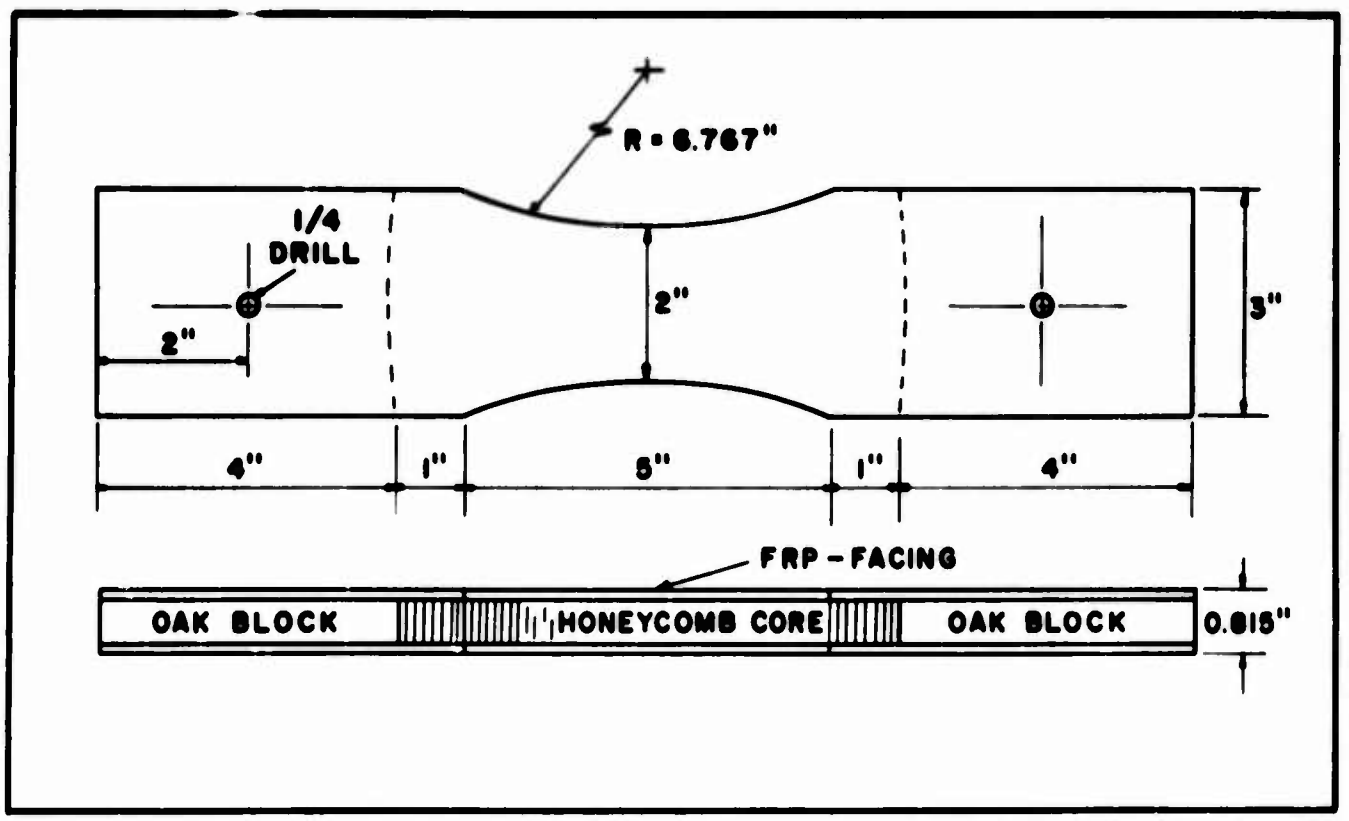

Figure 12. Fatigue Specimens. A, Kiln-Dried Oak Blocks To Prevent Core Crushing; B, Silver Plate Contact for Deflection Measurement; C, Honeycomb Core Material.

of 4 inches and kiln-dried oak blocks were glued between the facing laminates with an epoxy resin (EPON A-6). All edges of the facing were ground or hand lapped to proper dimensions to eliminate scratches and other imperfections which might affect the fatigue results. Two holes were drilled in the ends of the specimen for alignment in the fatigue machine.

All the specimens had a smooth glassy finish with very few imperfections visible to the eye. Microscopic examination, however, shows scattered small air inclusions a few thousandths of an inch in diameter. On occasion these were at the surface of the facing, resulting in small pick holes. These small imperfections were not uniformly distributed in all specimens and probably provided stress concentrations which had an undetermined effect on the fatigue life of each specimen. This matter is discussed later.

b. Fatigue Testing Equipment

Fatigue Electromagnetic Equipment. The fatigue equipment was designed around a Model C-10E vibration exciter manufactured by MB Manufacturing Company, Division of Textron, Inc. The exciter was fitted with a special flexure device, bolted to its top, which held the specimen. The general set-up is shown in Figure 13.

The Model C-10E exciter (A in the figure) provides a reciprocating movement by means of an induced electromagnetic force. The basic internal structure consists of a stationary field coil and a driver coil attached to the moving table. The table is mounted in a series of restraining rockers and rubber mounts such that a linear vertical motion is provided. The exciter has a capacity of 1200 pounds force for continuous-duty sinusoidal input with a maximum amplitude of 1 inch or a maximum velocity of 70 inches per second. The frequency range is 5 to 3,000 cps.

The C-10E exciter is controlled by a Model T151 electronic amplifier (B in Figure 13). This consists of a Model T104A automatic vibration exciter control, a power amplifier, and a DC field supply. The R104A unit consists of an oscillator, a frequency sweep unit, a vibration meter, an automatic level control, and an automatic displacement-acceleration transfer unit. Although there are many automatic features to this equipment, manual control and adjustment were used for these experiments.

The frequency of operation was monitored through a Hewlett-Packard Company Model 521G frequency counter, accurate to the nearest cycle per second. The counter was plugged directly into the T151 console unit.

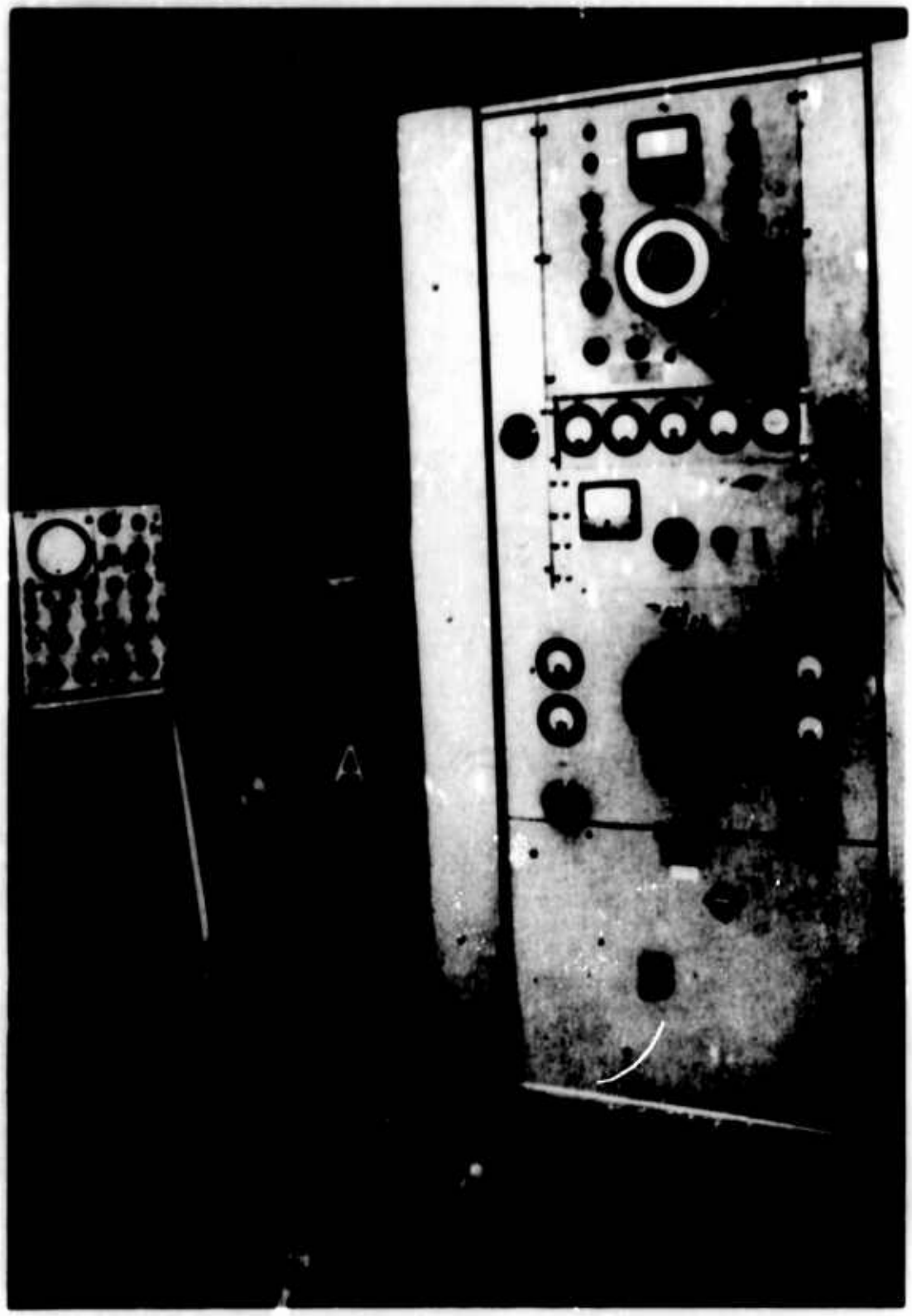

Figure 13. General View of Fatigue Testing Apparatus. A, C-10E Electromagnetic Exciter; B, T151 Control Console; C, Fatigue Device Bolted to the C-10E Exciter.

The fatigue device was specially designed and built from aluminum to mount on top of the C-10E exciter. It is shown in Figure 14 with a specimen clamped in place. Basically, this provides a simple beam with the link-type vertical end-supports (A in Figure 14) bolted to a large steel ring which in turn is bolted to the exciter frame. The load is applied through two sets of center links (B in Figure 14) bolted to the moving table of the exciter. Each link end was fitted with heavy-duty roller bearings. Because the four set of links supporting the specimen clamps provide a statically unstable force system, one set of rigid links (no lower bearings) coupled to a stabilizer bar (C in Figure 14) was necessary to eliminate side sway during operation.

The specimen was clamped in the mountings (D in Figure 14) supported by the vertical links. Vertical pins in these mounts assured proper alignment by fitting into accurately drilled holes in the specimen. One pin was extracted after specimen installation in order to eliminate any axial forces on the specimen. Clamping in the mounts was accomplished by a top plate secured with four cap screws. Each of the top plates was also fitted with four shear pins to insure that the clamps functioned as rigid bodies. The clamps (mounts and top plates) were lined with 1/32-inch-thick replaceable rubber sheets to prevent abrasion of the clamped portion of the specimens. All cap screws were torqued to 100 inch-pounds at the beginning of each test to provide uniform mounting conditions for the specimens. As stated previously, the specimens (H in Figure 14) were 15 inches long with 4 inches clamped at each end, leaving a 7-inch test zone loaded under a constant-type bending moment diagram (no shear).

An Endevco Model M2110 piezoelectric dynamic force gage with the accuracy of ± 1 per cent (E in Figure 14) was mounted in the rigid set of loading links to measure one of the reactions. The signal from the force gage was fed into a cathode follower amplifier for impedance matching and thence to a Tektronix oscilloscope (D in Figure 13) for read-out. This system was used to maintain a constant maximum force at the specimen loading points throughout a test by manual adjustment of the exciter control.

Dynamic deflections were measured by a micrometer gage (F in Figure 14) mounted on a stanchion which straddled the specimen at its centerline. A small copper spring with a silver tip was fitted to the end of the micrometer. While the specimen was vibrating, the spring tip was lowered to make contact with a small silver plate (3/16 inch by 3/16 inch in size, see B in Figure 12) held on the specimen with an adhesive at the point where deflection measurements were required.

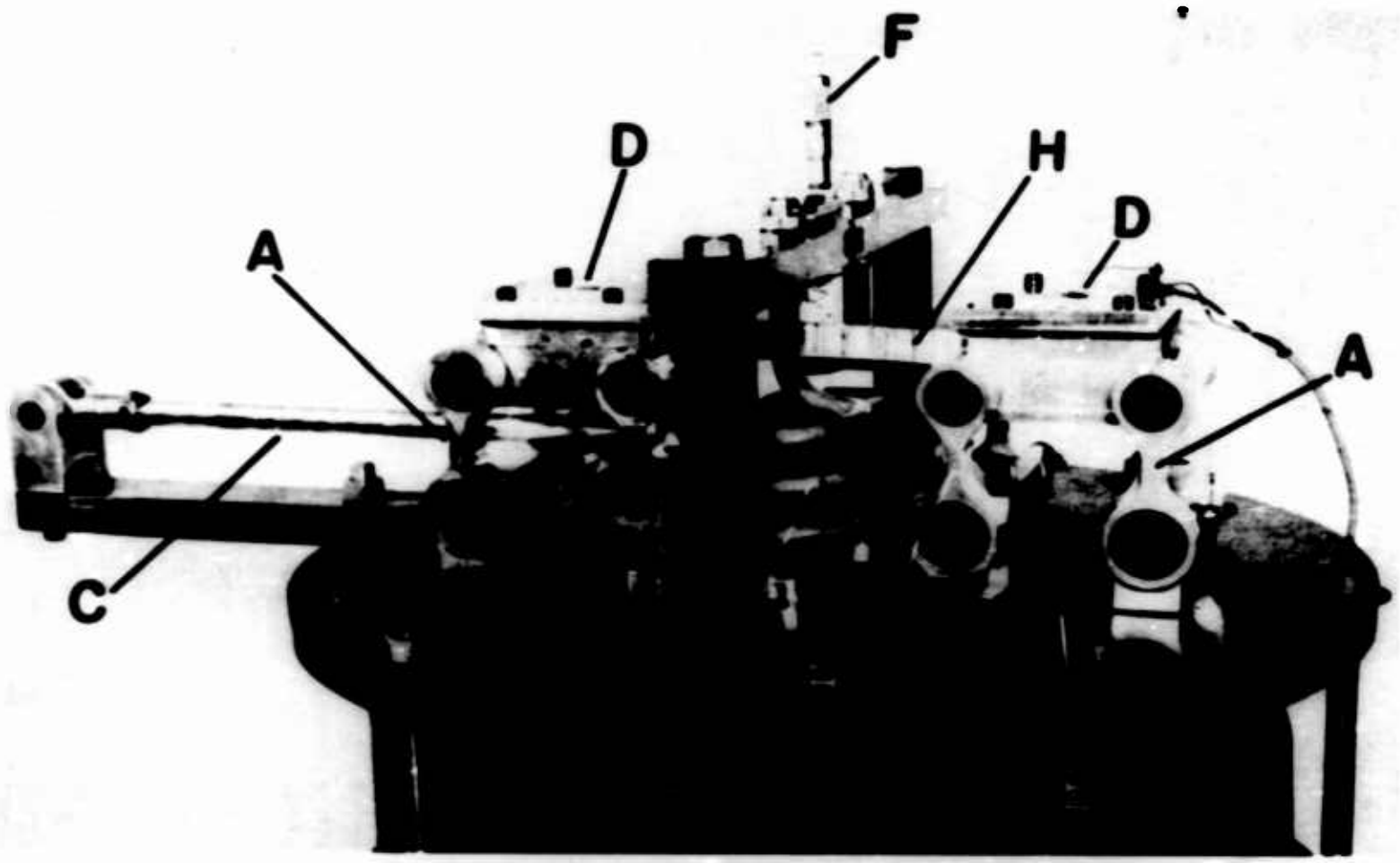

Figure 14. Detail View of the Fatigue Testing Device Mounted on the MB C-10E Exciter. A, End Support Links; B, Loading Links; C, Stabilizing Bar; D, End Clamps; E, Force Gage; F, Micrometer Dynamic Deflection Gage; G, Auxiliary Springs; H, Specimen.

Contact between the spring tip and the silver plate on each cycle of vibration completed a simple series circuit, the signal of which was displayed on an oscilloscope. This provided a simple visual mechanism to measure the dynamic maximum deflections with an accuracy of 0.001 inch.

Dynamic Strain Equipment. The dynamic strain-gage circuit for the fatigue tests was integrated with that used for the damping measurements described in section A2b. By a set of switches the strain measurements could be made on either the damping specimens or the fatigue specimens. As previously stated, the system included an AC bridge circuit, an AC amplifier, and an oscilloscope.

A carrier frequency of 1,000 cps was determined to be the optimum for the fatigue circuitry. The signal on the oscilloscope thus consisted of the amplified carrier signal on which was superimposed the dynamic strain signal from the specimen. As for the damping program, calibration of the oscilloscope trace was accomplished by shunting a strain gage with a resistor simulating strain.

During a test it was necessary to read the scope visually while adjusting the amplitude of the C-10E exciter, and this in itself led to significant errors because of the small variations possible on the displayed carrier wave. At the higher specimen facing stresses of 20,000 to 25,000 psi, reading accuracy could only be $\pm$10 per cent. At the lower stresses, because of smaller changes in the carrier signal, the error was increased to $\pm$20 per cent.

There were also considerable problems with the strain gages. Often the life of the strain gage under these severe loading conditions was so short (a few thousand cycles) that there was insufficient time to relate the strain measurements to the force-gage signal. A variety of adhesives, types of strain gages, and techniques of application were tried, but either the gages had a short life or the adhesive allowed the gage to yield relative to the facing material. This method was abandoned after testing ten specimens because of the difficulty encountered and the unreliability of the results. These specimens are not reported herein.

Static Loading Equipment for Fatigue Specimens. As an alternate solution to dynamic facing strain measurements, dynamic deflection measurements were taken by the micrometer gage previously described. The procedure followed consisted of relating the dynamic deflection to the force-gage reading while the test was running. Since the force-gage reading could be displayed full

scale on the scope, the force could be read with an accuracy of ±2.5 per cent, a considerable improvement over the strain-gage method.

In order to establish the relation between the deflection and the facing strain, a special testing device was made to load the fatigue specimens statically. The equipment employed, including the Instron testing machine, is shown in Figure 15. The configuration of the apparatus was identical to the fatigue device mounted on the C-10E exciter except for the fittings required for attachment to the Instron. Again, each end of the specimens was gripped between a mount and a top plate, both lined with 1/32-inch-thick rubber pads and screwed together with cap screws, and each torqued to 100 inch-pounds.

Deflections were measured by a Baldwin Model PD-1M differential transformer type deflectometer and automatically plotted versus load on the Instron x-y recorder (F in Figure 15), an integral part of the Instron machine. At the same time, stresses were read by a Baldwin digital strain recorder (G in Figure 15). The load versus deflection curve on the Instron chart was blipped at the desired points, and thus complete deflection versus facing strain data were accumulated.

c. Experimental Procedure

In constructing a fatigue S-N curve, the investigator is faced with a mismatch between the designer's needs and the limitations of laboratory fatigue equipment. The designer's needs are dictated by the loading requirements on the structure which he translates into the required stress capability. Thus, the S-N curve (stress versus number of cycles of load) is the type of information required for design.

The investigator finds it difficult to keep a constant stress in the specimens in the laboratory during the repeated load in certain cases. He may impose constant repetitive deflections or constant repetitive strains, but these may not be translated directly into stresses unless the material properties and geometry of the specimen remain unchanged during the test. This is not usually a problem in tests involving direct tension or compression repetitive loads, because with fixed specimen geometry and the capability of maintaining constant repetitive loads on the specimens, there will be repetition of a constant maximum stress even if the modulus of elasticity varies over the duration of the test.

In the case of this experiment, the specimens were flexure specimens and the methods of maintaining constant stress are indirect.

Figure 15. Equipment for Statically Loading Fatigue Specimens. A, Clamps to Grip Specimen; B, Fatigue Specimen; C, End Supports (Links); D, Loading Links; E, Baldwin Differential-Transformer Deflectometer; F, X-Y Recorder on Instron Testing Machine; G, Baldwin Digital Strain Recorder.

It is known that the modulus E of the fiberglass laminate facing materials changes with the number of cycles of stress. In tests reported herein, the modulus decreased as much as 35 per cent over the specimen life. Thus, if constant repetitive deflections are imposed on the specimen, the stress will decrease with the decreasing modulus E over the duration of the test. An alternative is that of tracking the strain on the specimen, but since converting strain information into stresses is also dependent upon the varying modulus, this could not be obtained without excessively complicating the instrumentation and running a separate investigation on modulus variation. Time would not permit this extra phase in the present investigation.

This problem was circumvented by a combination of strain, deflection and load measurements. In the feasibility portion of the experiment, two methods were used and evaluated. One method related dynamic strain-gage measurements to the force-gage readings, and the other method related dynamic deflection measurements to the force-gage readings.

In the strain-gage method, the amplitude of vibration of the machine was rapidly increased, thus increasing the deflection of the fatigue specimen, and at the same time the dynamic strain signal on the oscilloscope was read. This was an exceedingly tricky procedure. When the proper strain was achieved, the oscilloscope was switched to the force-gage circuit, and a force reading taken and then maintained throughout the duration of the test. Because of the difficulty in obtaining accurate strain readings (see second part of section B2b) and also maintaining strain gages serviceable for a long enough period to make the switch to the force gage, this method was abandoned.

As an alternate solution, one which proved to be much more feasible and accurate, a dynamic deflection measurement was made while the amplitude of vibration was rapidly increased. When the proper deflection was achieved (measured with an accuracy of 0.001), a force-gage reading was taken and then maintained for the duration of the test. The dynamic deflection measurement was previously described, on page 47.

In order to carry out this procedure, a relationship between deflection and facing stress had to be established. To do this, three specimens for each type of sandwich construction (aluminum or HRP core) were tested statically in the static loading device previously described (last part of section B2b). The fixture provided, as near as possible, identical conditions of clamping and load application to that which the fatigue equipment would give.

In each test the specimen was loaded to approximately 30 per cent of the ultimate flexural load to seat the specimen in the test fixture and to remove initial discontinuities from the deflection curve. The specimen was then loaded continuously at a rate of 0.05 inch per minute until a strain equivalent to 25,000 psi stress was recorded on the facings. Complete strain, deflection and load data were taken. The curve was re-run four times for each specimen, and on the final run the specimen was loaded to failure. The final failure strain was recorded and converted to ultimate failure stress based on a modulus of elasticity of 3.33×10^6 psi. The modulus was an average value based on tension and compression tests carried out on a laminate made at the same time as the sandwich panels (see section A2a, page 3).

The data from the three specimens for each type of sandwich construction (a total of 12 stress-deflection curves) were averaged to establish the deflection-stress relationship. All the curves were almost identical, which was an indication of the careful fabrication and machining process which was used to make the specimens. Nevertheless, the averaging of the results did perhaps serve to eliminate some minor experimental error and minor difference in specimens. The curves for both types of construction were also nearly identical. The following equations were obtained from the curves for use in calculating the dynamic stresses of the fatigue specimens:

Aluminum Core: Facing Stress (psi) = 7022 x deflection (inches)

HRP Core: Facing Stress (psi) = 7072 x deflection (inches).

It must be pointed out that there may be some indeterminate error in this process because the dynamic moduli and the static moduli may not be precisely the same. However, in section A3e it was concluded in the damping investigation that there was no significant difference between the two moduli for either of the core materials or the facing laminates at the rates of strain imposed in the damping vibrations. The rates of strain were estimated to be no more than three times as great in the fatigue tests as in the damping investigation, so that it is believed that the moduli are not significantly different. Nevertheless, this is the best relationship that could be established at this point.

A frequency of 40 cps was used for the fatigue test program. This frequency was chosen on the basis of the exciter's capability and a reasonable maximum speed for the specimen. At the highest stress (25,000 psi), a total vertical movement of the center of the specimen of over 0.7 inch was necessary, and the specimen could be observed only as a blur while under test. At this speed, the shortest failure time occurred in 5,743 cycles, or

only 2.4 minutes, while the longest tests made were 10 million cycles at 10,000 psi, or 72 hours of continuous operation. The fatigue machine required continuous monitoring and adjustment during each test.

The 40-cps operating frequency was near the resonance of the total mechanical system. The system consisted of two primary masses, the exciter table (approximately 20 pounds) and the fatigue device and specimen (approximately 15 pounds). A spring constant was provided by an internal spring, the specimen itself, and two auxiliary springs screwed to the table at the bottom and into the stanchion crossing above the specimen, which was in turn fastened to the frame of the exciter. The two auxiliary springs, each with a spring constant of 900 pounds per inch, were necessary to adjust the frequency of the system upwards to 40 cps and to give the system stability during the development of the fatigue process. Operating the system at resonance was favored to avoid overtaxing the exciter for the long test period, since this procedure would substantially reduce the force requirement.

It is emphasized that the system as a whole operated at resonance. There were no resonant effects on the specimen itself because its natural frequency would be in the vicinity of 800 cps or more in a simply supported state. Since both deflection and link-reaction force were measured dynamically, and even though the flexibility of the specimen increased over the duration of the test, constant repetitive moment was applied to the ends of the specimen; thus it may be stated that constant stress was achieved in the specimen facings throughout the duration of the test.

The deflection of the specimen increased as much as 35 per cent during a test. On a few specimens, dynamic deflection measurements were made periodically during the duration of the test. The test had to be a relatively long one (at least two hours) in order to record a sufficient number of points to plot a curve. In a test lasting only a few minutes there were too many required data to record and too many adjustments to make to take time for these extra data. Figure 16 shows a typical curve for deflection increase for a specimen (aluminum core) loaded at a facing stress of 14,000 psi.

Since only scant deflection increase data were taken, no comparison of deflection increase (decrease in modulus) can be made between stress levels or between specimens with the two types of core material. It was noted, however, that as the stiffness of the specimen decreased, the resonant frequency of the system changed and the exciter had to work harder to maintain constant force at the constant 40-cps frequency. This was apparent through

observations of the change of plate current required as displayed on the control console, indicating the change in input power. This, in fact, became a way of detecting approaching failure of specimens. When the plate current changed from a constant slow increase to a sharp increase requiring frequent adjustment of the vibration amplitude and reaction force, failure was imminent.

All the fatigue tests were run at ambient temperatures which ranged between 60 and 82 degrees Fahrenheit. Past research (reference 4) has shown little temperature effect on fatigue results for such small temperature variation. The specimens themselves became hotter than room temperature during the test due to energy absorption but became only warm to the touch. There seemed to be no detectable correlation between temperature and fatigue life.

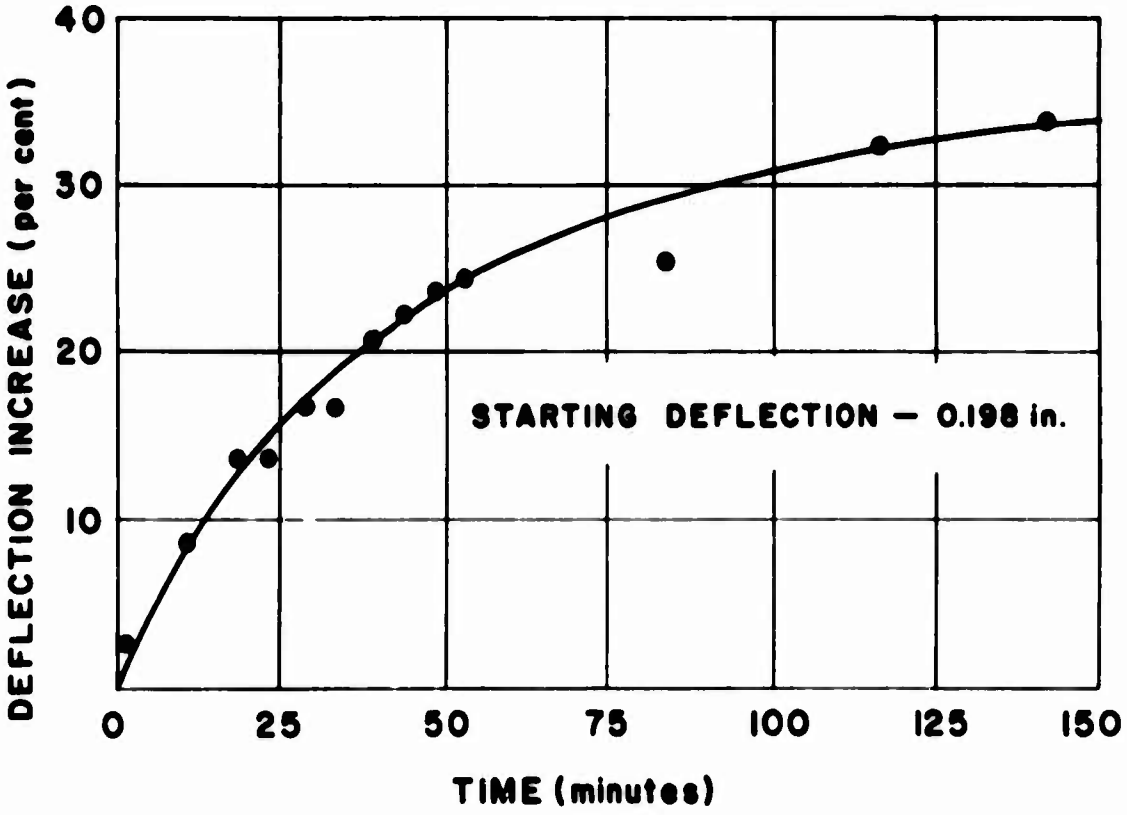

Figure 16. Typical Variation of Specimen Deflection with Time During Fatigue Testing. This specimen was constructed of HRP fiberglass core and was loaded 14,000 psi at the rate of 40 cps.

A total of 47 specimens were tested. Thirteen of these were experimental specimens used to adjust the equipment and standardize the procedures. One was used to check the effect of a particular "wave" form in the fabric due to an error in fabrication, and 33 were used to establish the S-N curve described later.

3. Test Results and Evaluation

a. S-N Curve and Discussion of Fatigue Data

Fatigue tests were run at the following six stress levels in the facing laminate: 25,000; 20,000; 17,000; 14,000; 12,000; and 10,000 psi. Three specimens were used to establish each point on the S-N curve for each type of sandwich construction tested, except for the 10,000 psi level where only three specimens were tested for both types. A summary of the results is shown in Tables 6 and 7 for each type of construction.

The numbers of cycles to failure at each stress level were averaged to plot the S-N curve. The resulting curve is presented in Figure 17. It will be noted in studying the data at each stress level that there is a considerable spread; yet, despite this spread in the data, the average value at each point falls on a smooth curve. The data for both the aluminum-core specimens and the HRP-core specimens seem to fall on the same curve; in fact, it did not seem feasible even to distinguish between the two materials in drawing the curve. This was not surprising because the type of flexure test used with constant moment on the test span gives only tension and compression in the facings with no shear stress in the core. However, there may have been some incidental uncalculable shear stress at the glue line or in the core due to small amounts of torsion or undetected unsymmetrical loading, but this would be minor compared with the flexural stresses.

All of the specimens failed in the fatigue machine except three. These included two aluminum-core specimens and one HRP-core specimen loaded at a facing stress of 10,000 psi. All of these endured 10 million cycles or more. It did not seem necessary to establish this point with more specimens since the S-N curve, if projected, indicated the life of a specimen loaded at 10,000 psi to be about 15 million cycles.

Although the curve seems to be gradually flattening, it does not necessarily indicate that the material has an endurance limit. Most nonmetallic materials do not have an endurance limit. The term fatigue strength is usually used in such cases and defines the stress that may be endured for a given number of cycles of load. From the curve, one can say the material has a fatigue strength at various numbers of cycles of load N as listed hereafter:

TABLE 6
FATIGUE TEST DATA - ALUMINUM CORE

Spec. No.	Fatigue Stress Level (psi)	Dynamic Deflection Imposed (in.)	Number of Cycles To Failure	Ratio of Fatigue Stress to Ult. Static Str***
A1	50,999	Static	1	-
A2	48,816	Static	1	-
A3	53,270	Static	1	-
Average	51,028			
A4	25,000	0.357	16,380	0.50
A5	25,000	0.357	7,398	
A6	25,000	0.357	8,232	
Average			10,670	
A7	20,000	0.285	33,424	0.40
A8	20,000	0.285	176,956	
A9	20,000	0.285	49,732	
Average			93,704	
A10	17,000	0.240	223,800	0.34
A11	17,000	0.240	254,760	
A12	17,000	0.240	135,300	
Average			203,953	
A13	14,000	0.199	1,039,200	0.28
A14	14,000	0.199	1,802,400	
A15	14,000	0.199	2,033,300	
Average			3,934,966	
A16	12,000	0.171	3,143,000	0.24
A17	12,000	0.171	3,233,300	
A18	12,000	0.171	5,428,600	
Average			3,934,966	
A19	10,000	0.142	10,159,200*	0.20
A20	10,000	0.142	10,000,000*	
Average			10,000,000	
A21**	14,000	0.199	609,600	

* Did Not Fail.

** Specimen Had Fabrication Error Introducing Wave Shape in Fill Direction.

*** Based on Average of Six Specimens - A1, A2, A3, F1, F2, and F3.

TABLE 7
FATIGUE TEST DATA - FIBERGLASS (HRP) CORE

Spec. No.	Fatigue Stress Level (psi)	Dynamic Deflection Imposed (in.)	Number of Cycles To Failure	Ratio of Fatigue Stress to Ult. Static Str***
F1	50,982	Static	1	-
F2	48,185	Static	1	-
F3	47,153	Static	1	-
Average	48,773			
F4	25,000	0.353	5,743	0.50
F5	25,000	0.353	6,062	
F6	25,000	0.353	15,395	
Average			9,068	
F7	20,000	0.283	105,522	0.40
F8	20,000	0.283	117,236	
F9	20,000	0.283	52,236	
Average			91,665	
F10	17,000	0.240	112,839	0.34
F11	17,000	0.240	359,580	
F12	17,000	0.240	165,600	
Average			212,673	
F13	14,000	0.198	2,034,145	0.28
F14	14,000	0.198	878,600	
F15	14,000	0.198	571,400	
Average			1,161,384	
F16	12,000	0.170	3,397,430	0.24
F17	12,000	0.170	4,081,506	
F18	12,000	0.170	3,797,600	
Average			3,758,835	
F19	10,000	0.141	10,000,000*	0.20

* Did Not Fail.

*** Based on Average of Six Specimens - A1, A2, A3, F1, F2, and F3.

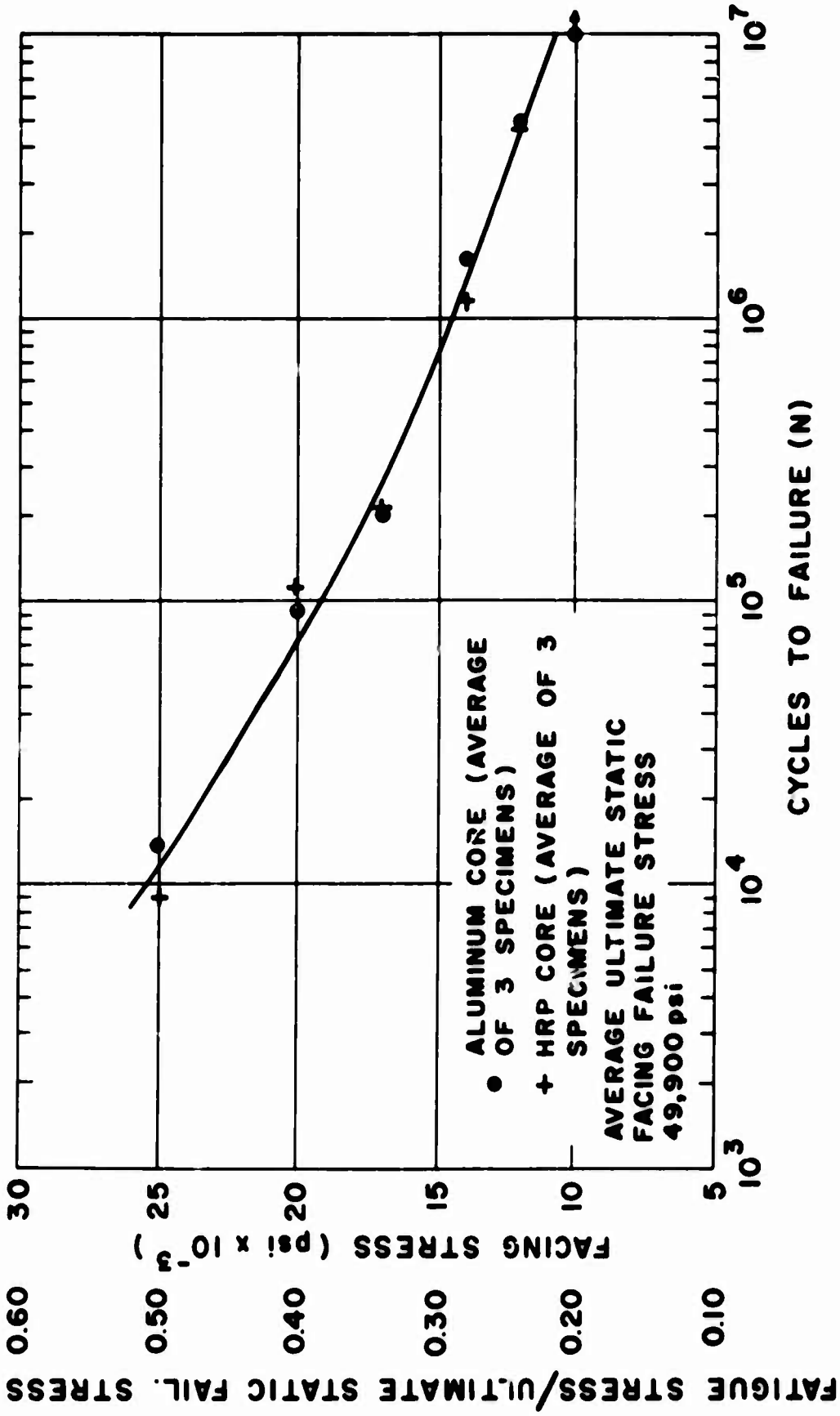

Figure 17. Fatigue S-N Curve for FRP Facing and Honeycomb Core Sandwich Structure Subjected to Pure Flexural Loading.

Fatigue Strength (psi)	Percent of Ultimate Strength	Number of Cycles (N)
19,000	38%	10^5
14,500	29%	10^6
10,000	20%	10^7 plus

b. Description of Types of Fatigue Failure

Figure 18 on the following page illustrates some typical fatigue failures. This is a group of aluminum-core specimens loaded at 14,000 psi in the facings. The failures were approximately perpendicular to the direction of the principal stress and followed the fabric fill direction (across the width direction). If the weave was slightly canted from perpendicular, the failure line followed the slant of the weave.

The majority of the failures occurred in the center "inch" of the specimens but rarely at the narrowest point. The point of failure seemed to be influenced by edge defects in some cases; i.e., after failure, four or five small cracks were noted extending into the center of some of the specimens a distance of approximately 1/32 inch from the edge, especially in the center inch of the specimen in an area adjacent to the failure line. All of these short cracks developed during the test, and apparently the most critical crack was rapidly propagated across the specimen at failure. At the high stresses, a sharp "report" was heard at failure as the crack propagated across the specimen in apparently one quarter cycle of load.

Simultaneously with the facing failure, the core material ruptured, with a vertical crack penetrating from the facing rupture to the opposite unruptured face. This is the only phase of the test where one type of core seemed to have superiority over the other. Here the aluminum core had only the vertical crack, while the HRP core became more shattered and the facing peeled from the core for about 1 to 2 inches back from the facing break due to acceleration forces in the fatigue machine. There were some diagonal cracks originating in or passing through the core perforations in some of the specimens. The cracks were at about 45 degrees. It was impossible to determine if these cracks were a function of the fatigue process similar to those reported by Apodaca and Preston (reference 50), where progressive cracking of core walls was reported, or if they were a function of the final rupture. At any rate, it appeared that the energy absorption characteristics of the aluminum core would thus be superior.

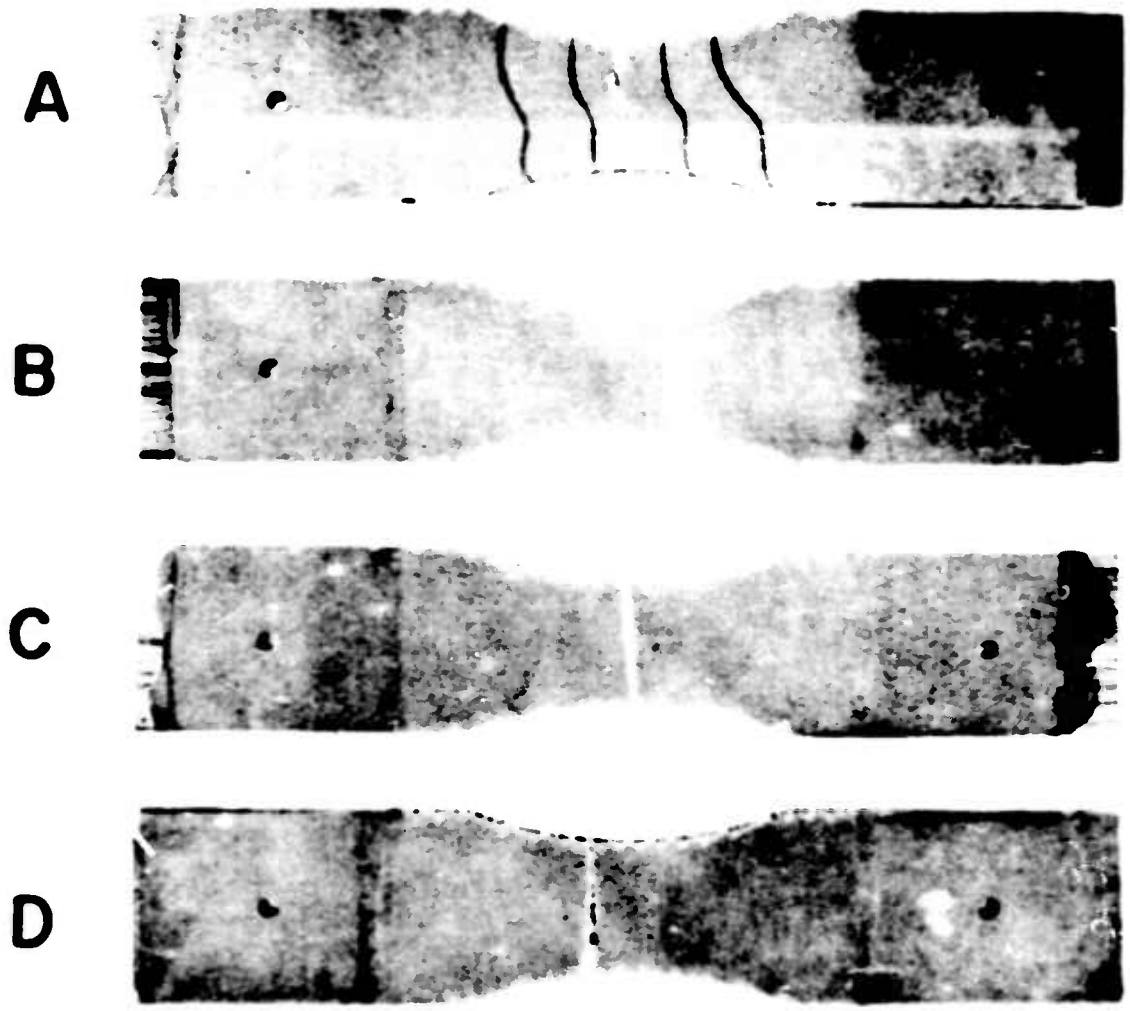

Figure 18. Typical Fatigue Failures Illustrated by the Family of Specimens Tested at 14,000 psi. A, Specimen A21 with "Wave" Fabrication Defect (Failed at 609,600 Cycles), Note Contours of Fill Line Drawn on Facing; B, C, and D, Specimens A13, A14, and A15 (Failing at 1,039,000; 1,802,400; and 2,033,300 Cycles).

Microscopic examination of the facing surface after failure showed a pattern of small microcracks. The cracks were perpendicular to the direction of the principal stress, following the fill direction of the fabric. The depth of cracks could not be determined, and they may not have penetrated beyond the first layer of fabric. It was not possible to observe with the microscope (100 power) the relationship of cracks to the cross-over points between the warp and fill strands because the strands are visually merged with the resin.

Apparently these microcracks have been observed before. Wilson (reference 48), for example, has reported the accumulation of interlaminar air blisters in filament-wound air-storage bottles cyclicly pressurized (4 cycles per minute) at as low as 3,000 cycles of pressure. These blisters could have been due to the formation of microcracks and the consequent penetration of the pressurized gas into the laminate. Broutmen (reference 7) also has studied these cracks for filament-wound plastics. He indicated that the cracks propagate to form larger cracks when the material is subjected to creep and fatigue loads and that these cracks can exist well in advance of ultimate fracture.

Scattered throughout the resin are small air bubbles ranging between 0.002 inch and 0.005 inch in diameter. These bubbles did not seem to influence the crack pattern; i.e., they were not the origin of the microcracks. Although sometimes cracks terminated in bubbles or passed through them, there were many bubbles which were bypassed by cracks. The bubbles were only faintly visible to the naked eye, and the surface of the specimens could usually be described as smooth and glossy. Some specimens exhibited more air bubbles than others, but there did not seem to be a relationship between the fatigue life and the number of air bubbles. On the contrary, some of the specimens with the greatest number of bubbles had the longest fatigue life.

The microcracks were spaced on the order of 1/64 inch to 1/32 inch or less and, when magnified, resembled a group of straws laid parallel to one another in a sort of lattice with very few perpendicular connections. The crack pattern was similar to the crack pattern observed in simple tension specimens. It could not be determined whether these cracks developed during the fatigue process or whether they were a function of the final failure process.

Werren (reference 47) has reported similar crazed formations in polyester laminates when tensile stresses beyond the initial proportional limit are applied. He hypothesizes that epoxide

laminates will probably craze also. Thus the resin gives less lateral support to the glass fibers on successive compressive loads, and failure may occur at a fewer number of cycles because of the more critical lateral buckling stresses in individual fibers.

It seems that more research should be done in the future on the formation of microcracks and the part they play in the fatigue process. Perhaps there are improvements in the weave or type of resin used which may eliminate them and, thus, increase fatigue life.

Specimen A in Figure 18 illustrates the failure of a specimen (A21, Table 6) which had a "wave" distortion of the fabric inadvertently produced in the fabrication process. Note that the failure line followed the "wave" fill line of the fabric. The fatigue life of this specimen was substantially below the average fatigue life of the other aluminum-core specimens in this group (14,000 psi): it endured only 38 per cent of the average fatigue life. Another similar specimen (A8, Table 6) was the highest in its group (17,000 psi), so that no conclusions can be drawn about such fabrication distortion defects.

c. Comparison of Results With Past Research

The only fatigue tests similar to those reported herein were performed by Keer and Lazan (reference 19). Only four specimens were reported on fiberglass facing-fiberglass core combinations, but several other types of sandwich constructions were reported. The tests were performed on an electromagnetic exciter with a double cantilever specimen mounted symmetrically on the machine. The specimen was vibrated at resonance, and a combination of flexure and shear was produced in the specimen instead of pure flexure as in the present tests. The four specimens established a smooth, but flat, S-N curve. All four specimens failed between 12,000 and 300,000 cycles of load at facing stresses ranging from 9,000 to 7,000 psi. None of the specimens in the tests given herein has such low fatigue life--at 10,000 psi, the lowest stress used, the life exceeded 10 million cycles.

No data on fabrication details were given, so that a direct comparison of results is impossible. In the resonant system used by Keer and Lazan, the natural frequency dropped off near failure as cracks developed. This gave more time to observe failure. The failures reported were similar to the tests reported herein; i.e., facing failure began with the breaking of many fibers of the facing (possibly similar to microcrack formation) and the development of a fragmented white portion

on the edge of the beam (delamination and edge crack) which moved toward the center, slowly at first, but finally resulting in a rapid failure. The frequency and load were maintained constant right up to failure in the tests reported herein, so that failure was quicker and of a more catastrophic nature. Other than having similar modes of failure, the tests do not seem to be comparable.

Other fatigue tests reported on sandwich construction are those by Werren (reference 46, parts C and H) and James and Norris (reference 17), both performed at the Forest Products Laboratory (FPL). All of these tests were aimed at core shear fatigue and were not comparable to the flexure tests reported herein. Nevertheless, some interesting conclusions were drawn which may affect the direction of USAAVLABS work. Both FPL investigations used heavier aluminum core. Werren used 3/8-inch cell size, perforated aluminum foil, 2 or 4 mils thick, laminated between 2024 clad aluminum alloy facings with a high temperature, thermoplastic, thermosetting resin. James and Norris used aluminum core with 3/8-inch cell size with 2-, 3-, or 4-mil thickness foil bonded directly to the test fixture. In both cases the glue line bonding the core to facings or fixture was generally unaffected by the fatigue loads early in the test, causing diagonal cracks in the core. This caused a slight load drop in the test, but did not cause failure. Final failure was a combination of diagonal cracks and buckling of core walls, with core-to-facing glue line failure as a secondary effect.

The James and Norris work indicated that the shear fatigue strength at 100,000 cycles averaged 40 per cent of the static shear strength. Also, the fatigue strength at low frequency (15 cps) was substantially higher than that obtained at high frequency (200 cps) by a factor of 1.75. The fatigue limit ranged from 20 to 23 per cent of static strength. Werren's results for aluminum core were higher, indicating a fatigue strength of 23 to 36 per cent of static strength at 30 million cycles of load depending on the plane of loading (ribbon direction or perpendicular to ribbon direction).

In a supplement to the first report, Werren (reference 46, part K) later reported more tests where core-to-facing bonds were more critical. However, given adequate bond, a fatigue strength of 38 per cent of the static strength could be expected at 30 million cycles of load. Since the core used in the tests reported herein was only 1 mil in thickness and had a density of no more than 50 per cent of those in the other investigations,

additional shear fatigue tests on aluminum core are needed. The investigation of the integrity of the core-to-facing bonds should also be a part of the program.

Werren (reference 46, part K) also tested fiberglass-honeycomb core laminated between 6-ply fiberglass facings or aluminum facings in shear fatigue in a similar method to that described above. The tests showed a fatigue strength at 30 million cycles of load of about 42 per cent of static strength. No weakness of glue line was indicated. Failures began by shear cracks either parallel or perpendicular to the flutes which gradually progressed during the test. The fatigue strength was affected very little by the direction of loading (ribbon direction or perpendicular to ribbon direction).

The only other fatigue tests on sandwich construction are those reported by Apodaca and Preston (reference 50). Several types of metal-honeycomb sandwiches were tested. A double cantilever specimen similar to Keer and Lazan's (reference 19) was tested at resonance in an electromagnetic vibrator. Thus, the specimen was subjected to both shear and flexure. The pertinent specimens used aluminum core material (5052-H39) with 3/16-inch cells and a 2-mil foil thickness. There was considerable scatter in the results, but a core shear fatigue strength of 27 per cent of the ultimate core shear strength was established at one million cycles. The shear fatigue strength found at the Forest Products Laboratory (reference 17 and 46) for pure shear is substantially higher than those reported by Apodaca and Presten. This leads to the hypothesis that flexure and shear combined loads will lead to shear fatigue failures at lower numbers of cycles of loads at a given core shear stress even if core shear fatigue failures are the final result. Thus, the area of combined flexure and shear fatigue loading needs further investigation.

There has been a great variety of fatigue tests on laminates of various thickness, types of fabric, and adhesives reported in the literature over the past few years (references 1, 4, 5, 7, 9, 21, 28, 32, 39, and 47 are a sample of these). Some of this work bears directly on the present results. Boller (reference 4) reported tests on a series of 23-ply fiberglass laminates using 181-Volan A fabric and alkyd-styrene or polyester adhesives. The results indicated a fatigue strength of 9,000 psi (FS/UTS = 0.22) at 10 million cycles and 20,600 psi (FS/UTS = 0.51) at 10,000 cycles. These results are slightly below the fatigue strength obtained in this project, but Pusey (reference 32) has indicated that polyester laminates are inferior to epoxy laminates in fatigue.

Werren (reference 47) and Kimball (reference 21), both Forest Products Laboratory investigators, supplemented Boller's work. The specimens were 24- or 26-ply tension-compression specimens of 181-Volan A fabric, with an EPON 828 and curing agent CL adhesive system. The tests were aimed at comparing notched specimens with unnotched specimens loaded at various angles to the warp direction. Several S-N curves reported by Werren seem to be comparable to the results reported herein for sandwich facings. The fatigue strength to ultimate static strength ratio ranged from 0.27 to 0.41 at 10 million cycles and 0.35 to 0.48 at one million cycles. The FPL results, whether expressed in ratio form or in psi, exceeded the fatigue strengths for the facings reported herein. Of course, this leads to the suspicion that there is a difference in failure mechanism between a 3-ply laminate and a 24- to 26-ply laminate or that the methods of tests are not comparable at all.

4. Conclusions and Recommendations

The major conclusions and recommendations drawn from the fatigue testing phase of the research are as follows:

a. The composite sandwich construction of the type tested does not have a fatigue endurance limit. Instead, a fatigue strength of the facings at a given number of cycles of load may be used to express its fatigue characteristics. For these tests the fatigue strength was 14,500 psi in the sandwich facings at one million load cycles.

b. There was considerable scatter in the results of the fatigue tests at a particular stress level due to the great number of variables present in composite sandwich construction. The average of the data at each stress level allowed the construction of a smooth S-N curve. When enough similar tests are made, the probability of failure should be included in the analysis and probability of failure versus cycles of load curve constructed for various stress levels.

c. All fatigue failures for fiberglass sandwich construction loaded in pure flexure will occur in the facings. The core material and glue line between core and fatigue were unaffected within the limits of the tests reported herein.

d. There was no difference in fatigue life between the fiberglass sandwiches using aluminum honeycomb core and those using HRP fiberglass honeycomb core.

e. Further research should be performed on the fatigue strength of the glue line between the facing laminate and the core material using the combination of materials reported in this research. Past research indicates that the glue line is not a problem for various other adhesive combinations, but this should be verified for the present material combinations.

f. Further research should be carried out on combination fatigue loading conditions; i.e., combinations of flexure and shear in sandwich construction, and biaxial loading of both laminates alone and as used in sandwich construction with various types of core material. This research should not be carried out until more fabrication research and static tests are performed on singly and doubly curved panels and on full-scale components.

g. At this point, it appears that the sandwich construction with aluminum honeycomb cores has a slight advantage over those using HRP fiberglass honeycomb cores. This opinion is based mostly on the more extensive damage done to the HRP core in the fatigue failure process even though both types fall on the same S-N curve.

h. Research on the development of microcracks and methods of preventing them is encouraged. Although some improvements can probably be made along these lines by changes in fabric, the main problem is probably in the molecular structure of the resin. Thus, the compatibility of resin with fiberglass will probably be improved mainly by changes in the adhesives and glass coatings.

i. The fatigue results are generally encouraging and compare favorably with previous tests reported for fiberglass laminates alone.

REFERENCES

1. Anderson, James A., and J. A. McCarthy, "Pre-preg Reinforced Plastics in Fatigue Applications," Proceedings, 18th Annual Technical and Management Conference, Reinforced Plastics Division, The Society of the Plastics Industry, Inc., February 1963, Section 8-C, pp. 1-8.

2. Anderson, R. A., "Flexural Vibrations in Uniform Beams According to the Timoshenko Theory," Journal of Applied Mechanics 20, Transactions of the American Society of Mechanical Engineers 75, 1953, pp. 504-510.

3. Bert, C. W., and W. S. Hyler, Design Considerations in Selecting Materials for Large Solid-Propellant Rocket-Motor Cases, Report Number 180, Defense Metals Information Center, Battelle Memorial Institute, Columbus, Ohio, 1962.

4. Boller, K. H., Fatigue Tests of Glass-Fabric-Base Laminates Subjected to Axial Loading, Report Number 1823, Forest Products Laboratory, Madison, Wisconsin, August 1958.

5. Boller, K. H., Supplement to Fatigue Tests of Glass-Fabric-Base Laminates Subjected to Axial Loading, Report Number 1823-A, Forest Products Laboratory, Madison, Wisconsin, April 1954.

6. Bresse, M., Cours de Mécanique Appliquée. Paris: Mallet-Bachelier, 1859.

7. Broutman, L. J., "Failure Mechanisms for Filament Reinforced Plastic Subjected to Static Compression, Creep and Fatigue," Proceedings, 19th Annual Technical and Management Conference, Reinforced Plastics Division, The Society of the Plastics Industry, Inc., February 1964, Section 9-C, pp. 1-10.

8. Clary, R. R., and S. A. Leadbetter, An Analytical and Experimental Investigation of the National Frequencies of Uniform Rectangular-Cross-Section Free-Free Sandwich Beams, Technical Note D-1967, National Aeronautics and Space Administration, 1963.

9. Cornish, R. H., H. R. Nelson, and J. W. Dally, "Compressive Fatigue and Stress Rupture Performance of Fiber Reinforced Plastics," Proceedings, 19th Annual Technical and Management Conference, Reinforced Plastics Division, The Society of the Plastics Industry, Inc., February 1964, Section 9-E, pp. 1-22.

10. Dar, S. M., "Vibrations of Rectangular Sandwich Plates With Various Edge Conditions," Unpublished Ph.D. Dissertation, University of Oklahoma, 1964.

11. Dengler, M. A., and M. A. Goland, "Transverse Impact of Long Beams Including Rotatory Inertia and Shear Effects," Proceedings of the First National Congress, Applied Mechanics, American Society of Mechanical Engineers, New York, 1951. pp. 179-186.

12. Dove, Richard C., and P. H. Adams, Experimental Stress Analysis and Motion Measurement, Charles E. Merrill Books, Inc., Columbus, Ohio, 1964

13. Glaser, A. R. "The Vibration of Sandwich Beams," Proceedings of the 7th Midwestern Mechanics Conference, Developments in Mechanics, Volume 1, Plenum Press, New York, 1961, pp. 228-238.

14. Hackman, L. E., R. J. Molella, C. L. Stotler, and D. G. Worthington, Structural Fiber Glass Aircraft Component-Program Results, Paper No. 64-442, American Institute of Aeronautics and Astronautics, 1964.

15. Huang, T. C., "The Effect of Rotatory Inertia and of Shear Deformation on the Frequency and Normal Mode Equations of Uniform Beams with Simple End Conditions," Journal of Applied Mechanics 28, Transactions of the American Society of Mechanical Engineers 83E, 1961, pp. 579-584.

16. James, William L., Calculation of Vibration Damping in Sandwich Construction from Damping Properties of the Cores and Facings, Report Number 1888, Forest Products Laboratory, Madison, Wisconsin, 1962.

17. James, William L., and Charles B. Norris, An Apparatus for Measuring Internal Friction and Fatigue Strength of Core Materials Used in Sandwich Construction, Report Number 1866, Forest Products Laboratory, Madison, Wisconsin, October 1958.

18. Kaman Aircraft Corporation, Compilation and Analysis of Test Data on Fiberglass-Reinforced Plastics, USATRECOM Technical Report 64-9, U. S. Army Transportation Research Command, Fort Eustis, Virginia, March 1964.

19. Keer, L., and B. J. Lazan, Damping and Fatigue Properties of Sandwich Configurations in Flexure, Technical Report 61-646, Aeronautical Systems Division, U. S. Air Force, November 1961.

20. Kimball, A. L., and D. E. Lovell, "Internal Friction in Solids," Physical Review, Series 2 vol. 30, 1927, pp. 948-959.

21. Kimball, K. E., Supplement to Fatigue Tests of Glass-Fabric-Base Laminates Subjected to Axial Loading-Effect of Notches, Report Number 1823-C, Forest Products Laboratory, Madison, Wisconsin, October 1958.

22. Kimel, W. R., M. E. Raville, P. G. Kirmser, and M. P. Patel, "Natural Frequencies of Vibration of Simply Supported Sandwich Beams," Proceedings of the 4th Midwestern Conference on Solid Mechanics, 1959, pp. 441-456.

23. Kobayashi, S., "On Vibration of Sandwich Beam," Proceedings of the 4th Japan National Congress of Applied Mechanics, Tokyo, 1954, pp. 369-372.

24. Kruszewski, E. T., Effect of Transverse Shear and Rotary Inertia on the Natural Frequency of a Uniform Beam, Technical Note 1909, National Advisory Committee for Aeronautics, 1949.

25. Lazan, B. J., Fatigue Failure Under Resonant Vibration Conditions, Technical Report 54-20, Wright Air Development Center, 1954. Also, American Society for Metals, Special Publication on Fatigue, 1954, pp. 36-77.

26. Mindlin, R. D., "Influence of Rotatory Inertia and Shear on Flexural Motions of Isotropic Elastic Plates," Journal of Applied Mechanics 18, Transactions of the American Society of Mechanical Engineers 73, 1951, pp. 31-38.

27. Mindlin, R. D., and H. Deresiewicz, "Timoshenko's Shear Coefficient for Flexural Vibrations of Beams," Proceedings of the Second U. S. National Congress on Applied Mechanics, American Society of Mechanical Engineers, 1954, pp. 175-178.

28. Nara, H. R., "Some Fatigue Characteristics of Glass-Reinforced Plastics," Proceedings, 12th Annual Technical and Management Conference, Reinforced Plastics Division, The Society of the Plastics Industry, Inc., February 1957, Section 5-D, pp. 1-6.

29. Nordby, Gene M., and W. C. Crisman, The Effect of Resin Content and Voids on the Strength of Fiberglass-Reinforced Plastics for Airframe Use, USAAVLABS Technical Report 65-66, U. S. Army Aviation Materiel Laboratories, Fort Eustis, Virginia, November 1965.

30. Nordby, Gene M., J. V. Noyes, and W. C. Crisman, Research in the Field of Fiberglass-Reinforced Sandwich Structure for Airframe Use, USATRECOM Technical Report 64-37, U. S. Army Transportation Research Command, Fort Eustis, Virginia, July 1964.

31. Plass, H. J., Jr., "Damping of Vibrations in Elastic Rods and Sandwich Structures by Incorporation of Additional Viscoelastic Material," Proceedings of the 3rd Midwestern Conference on Solid Mechanics, 1957, pp. 48-71.

32. Pusey, B. B., "Flexural Fatigue Strengths of Reinforced Thermosetting Laminates," Proceedings, 12th Annual Technical and Management Conference, Reinforced Plastics Division, Society of the Plastics Industry, Inc., February 1957, Section 5-C, pp. 1-10.

33. Raville, M. E., E.-S. Ueng, and M.-M. Lei, "Natural Frequencies of Vibration of Fixed-Fixed Sandwich Beams," Journal of Applied Mechanics 28, Transactions of the American Society of Mechanical Engineers 83E, 1961, pp. 376-381.

34. Rayleigh, J. W. S., The Theory of Sound, First edition, 1877; American edition, Dover Publications, New York, 1945.

35. Reissner, E., "The Effect of Transverse Shear Deformation on the Bending of Elastic Plates," Journal of Applied Mechanics 12, Transactions of the American Society of Mechanical Engineers 67, 1945, A69-A77.

36. Richter, H. P. H., "Photographic Method for Measuring Material Damping and Dynamic Youngs Modulus at Low Frequencies Applied to A Fiberglass Reinforced Resin Structure," Proceedings, 18th Annual Technical and Management Conference, Reinforced Plastics Division, The Society of the Plastics Industry, Inc., February 1963, Section 4-D, pp. 1-10.

37. Ross, D., E. E. Ungar, and E. M. Kerwin, Jr., "Damping of Plate Flexural Vibrations by Means of Viscoelastic Laminae," Structural Damping, American Society of Mechanical Engineers, 1959.

38. "Sandwich Constructions and Core Materials; General Test Methods," MIL-STD-401A, Military Standard, June 1956.

39. Stevens, G. H., Fatigue Test of Phenolic Laminate at High Stress Levels and Elevated Temperatures, Report Number 1884, Forest Products Laboratory, Madison, Wisconsin, 1961.

40. Timoshenko, S. P., "On the Correction for Shear of the Differential Equation for Transverse Vibrations of Prismatic Bars," Philosophical Magazine, 41, 6th series, 1921, pp. 742-746.

41. Timoshenko, S. P., "On the Transverse Vibration of Bars of Uniform Cross-Section," Philosophical Magazine 43, 6th series, 1922, pp. 125-131.

42. Timoshenko, S. P., Vibration Problems in Engineering, Third edition, Princeton, N. J.; D. Van Nostrand Company, Inc., 1955.

43. Timoshenko, S. P., and J. N. Goodier, Theory of Elasticity, 2nd edition, McGraw-Hill Book Company, Inc., New York, 1951, pp. 452.

44. Traill-Nash, R. W., and A. R. Collar, "The Effect of Shear Flexibility and Rotatory Inertia on the Bending Vibrations of Beams," Quarterly Journal of Mechanics and Applied Mathematics 6, 1953, pp. 186-222.

45. Ungar, E. E., "Highly Damped Structures," Machine Design 36 (4), February 14, 1963, pp. 162-168.

46. Werren, Fred, Fatigue of Sandwich Constructions for Aircraft, Report Numbers 1559C, 1559D, 1559E, 1559H, 1559I, 1559K and 1559L, Forest Products Laboratory, Madison, Wisconsin, 1948-52.

47. Werren, Fred, Supplement to Fatigue Tests of Glass-Fabric-Base Laminates Subjected to Axial Loading, Report Number 1823-B, Forest Products Laboratory, Madison, Wisconsin, August 1956.

48. Wilson, Frank M., "Development of Fatigue-Resistant Filament-Wound Emergency Air Storage Bottles," Proceedings, 19th Annual Technical and Management Conference, Reinforced Plastics Division, The Society of the Plastics Industry, Inc., Febrary 1964, Section 1-E, pp. 1-3.

49. Yu, Y. -Y., "Damping of Flexural Vibrations of Sandwich Plates," Journal of the Aerospace Sciences, Volume 29, 1962, pp. 790-803.

50. Apodaca, D. R., and J. L. Preston, Fatigue in Shear by Bending of Structural Sandwich Constructions, Technical Report Number ASD-TR-61-338, Aeronautical Systems Division, Wright-Patterson Air Force Base, Ohio, March 1963.

APPENDIX

FREQUENCY AND MODE-SHAPE ANALYSIS BY TIMOSHENKO BEAM THEORY

A complete derivation of the Timoshenko beam theory for vibration of homogeneous beams with flexural and shear flexibility and lateral (translational) and rotatory inertia is developed here from first principles. This was deemed necessary for the following reasons:

(1) The most complete Timoshenko beam vibration analysis reported in the literature (Huang, reference 15) contains some minor errors.

(2) Inclusion of this derivation makes the complete and correct analysis available without resorting to numerous references.

(3) It will be used as the basis for sandwich beam calculations discussed in section A3c.

Derivation of the Differential Equation of Motion for a Timoshenko Beam

The Lagrangian method is used here to derive the governing partial differential equation. For a derivation using Newton's second law, the reader is referred to pp. 329-331 of reference 42.

All energies are per unit length of beam. The strain energy of bending is

$$(1/2)EI\left(\partial\psi/\partial x\right)^2$$

where E is the elastic modulus of the facings, I is the area moment of inertia about the neutral axis, ψ is the slope of the beam deflection curve due to flexure only, and x is the position co-ordinate along the length of the beam.

The strain energy of transverse shear deformation is

$$(1/2)AKG\left(\frac{\partial y}{\partial x} - \psi\right)^2$$

where A is the shear area, K is a shear-deformation shape factor to be determined in a later section, G is the core modulus of elasticity in shear, and y is the total lateral deflection.

The translational kinetic energy is

$$(1/2)\ M\ (\partial y/\partial t)^2$$

where M is the total beam mass per unit length of beam and t is time. The rotational kinetic energy is

$$(1/2)\ J\ (\partial \psi/\partial t)^2$$

where J is the total beam mass moment of inertia per unit length of beam. Then twice the Lagrangian is given by

$$M\ (\partial y/\partial t)^2 + J\ (\partial \psi/\partial t)^2 - EI\ (\partial \psi/\partial x)^2 - GAK\left(\frac{\partial y}{\partial x} - \psi\right)^2 .$$

Applying Hamilton's principle to the Lagrangian results in the following set of partial differential equations:

$$M\frac{\partial^2 y}{\partial t^2} - GAK\left(\frac{\partial^2 y}{\partial x^2} - \frac{\partial \psi}{\partial x}\right) = 0 \quad \text{(A-1)}$$

$$J\frac{\partial^2 \psi}{\partial t^2} - EI\frac{\partial^2 \psi}{\partial x^2} - GAK\left(\frac{\partial y}{\partial x} - \psi\right) = 0. \quad \text{(A-2)}$$

Solving Equation (A-1) for ψ:

$$\psi = \int\left(\frac{\partial^2 y}{\partial x^2} - \frac{M}{GAK}\frac{\partial^2 y}{\partial t^2}\right) dx = \frac{\partial y}{\partial x} - \int \frac{M}{GAK}\frac{\partial^2 y}{\partial t^2}\, dx .$$

Putting this into Equation (A-2) gives

$$J\frac{\partial^3 y}{\partial x \partial t^2} - \frac{JM}{GAK}\int\frac{\partial^4 y}{\partial t^4} dx - EI\frac{\partial^3 y}{\partial x^3} + \frac{EIM}{GAK}\frac{\partial^3 y}{\partial x \partial t^2} - GAK\int \frac{M}{GAK}\frac{\partial^2 y}{\partial t^2} dx = 0 .$$

Now, differentiating with respect to x to eliminate the integrals results in

$$EI\frac{\partial^4 y}{\partial x^4} + M\frac{\partial^2 y}{\partial t^2} - \left(J + \frac{EIM}{GAK}\right)\frac{\partial^4 y}{\partial x^2 \partial t^2} + \frac{JM}{GAK}\frac{\partial^4 y}{\partial t^4} = 0$$

or

$$\frac{\partial^4 y}{\partial x^4} + \frac{M}{EI}\frac{\partial^2 y}{\partial t^2} - \left(\frac{J}{EI} + \frac{M}{GAK}\right)\frac{\partial^4 y}{\partial x^2 \partial t^2} + \left(\frac{J}{EI}\right)\left(\frac{M}{GAK}\right)\frac{\partial^4 y}{\partial t^4} = 0 . \quad \text{(A-3)}$$

Equation (A-3) is equivalent to an equation derived by Timoshenko for a homogeneous beam. The application of Equation (A-3) to sandwich-type beams is presented in section A3d.

In similar fashion, the following equation in ψ can be written:

$$\frac{\partial^4\psi}{\partial x^4} + \frac{M}{EI}\frac{\partial^2\psi}{\partial t^2} - \left(\frac{J}{EI} + \frac{M}{GAK}\right)\frac{\partial^4\psi}{\partial x^2\,\partial t^2} + \left(\frac{J}{EI}\right)\left(\frac{M}{GAK}\right)\frac{\partial^4\psi}{\partial t^4} = 0 \quad \text{(A-4)}$$

General Solution of the Timoshenko Beam Equation

Due to the presence of the term containing the mixed partial derivative in Equation (A-3), the x and t variables do not separate exactly in the general free-vibration case. However, in the present research program, the beam is first excited sinusoidally and then the excitation is cut off. Under these conditions, it appears to be a very reasonable approximation to assume a sinusoidal wave form shape with respect to time, as follows:

$$y = Y(x)\sin\omega t \quad \text{(A-5)}$$

where ω is the frequency and Y (x) is the modal shape of the beam deflection curve (to be determined). It should be mentioned that so far as is known, all previous investigators of both Timoshenko-beam and sandwich-beam vibrations have made an assumption equivalent to Equation (A-5).

Substitution of Equation (A-5) into Equation (A-3) gives

$$Y^{iv} - \frac{M\omega^2}{EI}Y + \left(\frac{M}{GAK} + \frac{J}{EI}\right)\omega^2 Y'' + \frac{JM\omega^4}{EIGAK}Y = 0 \quad \text{(A-6)}$$

where the primes denote differentiation with respect to x.

Equation (A-6) can be rearranged as follows:

$$Y^{iv} + \left(\frac{M}{GAK} + \frac{J}{EI}\right)\omega^2 Y'' - \frac{M\omega^2}{EI}\left(1 - \frac{J\omega^2}{GAK}\right)Y = 0 \quad . \quad \text{(A-7)}$$

Equation (A-7) will now be nondimensionalized and solved following the notation used by Huang (reference 15). First, the following dimensionless parameters are introduced:

Position parameter	$\epsilon = x/L$	(A-8)
Bending flexibility parameter	$b^2 = \frac{ML^4}{EI}\omega^2$	
Rotatory inertia parameter	$r^2 = J/ML^2$	
Shear flexibility parameter	$s^2 = EI/GAKL^2$	

Then Equation (A-7) becomes

$$Y^{iv} + b^2 (r^2 + s^2) Y'' - b^2 (1 - b^2 r^2 s^2) Y = 0 \qquad \text{(A-9)}$$

where now the primes denote differentiation with respect to ϵ.

In similar fashion, the solution of Equation (A-4) can be assumed to be of the form

$$\psi = S(x) \sin \omega t . \qquad \text{(A-10)}$$

Then, following the identical procedure used above to obtain Equation (A-9), the following result is obtained:

$$S^{iv} + b^2 (r^2 + s^2) S'' - b^2 (1 - b^2 r^2 s^2) S = 0 . \qquad \text{(A-11)}$$

The solutions of Equations (A-9) and (A-11) can be written as follows:

$$Y = C_1 \cosh b\alpha\epsilon + C_2 \sinh b\alpha\epsilon + C_3 \cos b\beta\epsilon + C_4 \sin b\beta\epsilon \qquad \text{(A-12)}$$

and

$$S = C_1' \sinh b\alpha\epsilon + C_2' \cosh b\alpha\epsilon + C_3' \sin b\beta\epsilon + C_4' \cos b\beta\epsilon \qquad \text{(A-13)}$$

where

$$\alpha = (1/\sqrt{2}) \left\{ - (r^2 + s^2) + \left[(r^2 - s^2)^2 + (4/b^2) \right]^{1/2} \right\}^{1/2} \qquad \text{(A-14)}$$

$$\beta = (1/\sqrt{2}) \left\{ (r^2 + s^2) + \left[(r^2 - s^2)^2 + (4/b^2) \right]^{1/2} \right\}^{1/2} . \qquad \text{(A-15)}$$

In writing the solutions in the form of Equations (A-12) and (A-13), it is necessary to assume that

$$\frac{\left[(r^2 - s^2)^2 + (4/b^2) \right]^{1/2}}{r^2 + s^2} > 1 . \qquad \text{(A-16)}$$

For the sandwich beams used in this project, the inequality (A-16) is satisfied for all frequencies below approximately 10,800 cps, which is well above the highest natural frequency obtained in the project.

The modal shape functions given by Equations (A-12) and (A-13) involve eight unknown constants of integration. However, only four boundary conditions (two at each end) can be written for a given simple beam configuration. Thus, some additional relationships among the coefficients

must be found. To do this, Equations (A-5) and (A-10) are substituted into Equation (A-1) with the following result:

$$Y'' + b^2 s^2 Y - LS = 0 . \qquad \text{(A-17)}$$

Substituting solutions Y and S as given by Equations (A-12) and (A-13) into Equation (A-17) gives the following four relationships:

$$\begin{aligned} C_1/C_1' = C_2/C_2' &= (L/b\alpha)\ \left[1 - b^2 s^2\ (\alpha^2 + r^2)\right] \\ -C_3/C_3' = C_4/C_4' &= (L/b\beta)\ \left[1 + b^2 s^2\ (\beta^2 - r^2)\right] . \end{aligned} \qquad \text{(A-18)}$$

Equations (A-12), (A-13), and (A-18) are identical to those obtained by Huang. When used in conjunction with appropriate boundary conditions, these equations allow solution for the natural frequencies.

Solution for a Simple Free-Free Timoshenko Beam

As first pointed out by Dengler and Goland (reference 11), the correct boundary conditions for a free end are as follows:

$$\frac{\partial \psi}{\partial x} = 0 \qquad \text{(A-19)}$$

and

$$\frac{\partial Y}{\partial x} - \psi = 0 . \qquad \text{(A-20)}$$

Equation (A-19) states that the curvature due to bending is zero, while Equation (A-20) states that the shear deformation is zero. Applying Equations (A-19) and (A-20) at both ends of the free-free beam ($\epsilon = 0$ and $\epsilon = 1$) gives the following four boundary conditions in terms of the modal functions Y and S:

$$\begin{aligned} S'(0) &= 0 & Y'(0) - LS(0) &= 0 \\ S'(1) &= 0 & Y'(1) - LS(1) &= 0 . \end{aligned} \qquad \text{(A-21)}$$

Substitution of Equations (A-12) and (A-13) into boundary conditions (A-21) results in the following set of simultaneous equations:

$$\begin{aligned} \alpha C_1' + \beta C_3' &= 0 \\ \alpha C_1' \cosh b\alpha + \alpha C_2' \sinh b\alpha + \beta C_3' \cos b\beta - \beta C_4' \sin b\beta &= 0 \\ (b/L)\ (\alpha C_2 + \beta C_4) - C_2' - C_4' &= 0 \end{aligned} \qquad \text{(A-22)}$$

$$(b\alpha/L)\,(C_1 \sinh b\alpha + C_2 \cosh b\alpha) - (b\beta/L)\,(C_3 \sin b\beta - C_4 \cos b\beta) - C_1' \sinh b\alpha - C_2' \cosh b\alpha - C_3' \sin b\beta - C_4' \cos b\beta = 0 \,. \tag{A-22}$$

Using Equations (A-18) to convert the unprimed coefficients in Equations (A-22) to primed ones results in the following set of four equations in the four primed coefficients:

$$\begin{aligned}
\alpha C_1' + \beta C_3' &= 0 \\
\alpha C_1' \cosh b\alpha + \alpha C_2' \sinh b\alpha + \beta C_3' \cos b\beta - \beta C_4' \sin b\beta &= 0 \\
-(\alpha^2 + r^2)\, C_2' + (\beta^2 - r^2)\, C_4' &= 0 \\
-(\alpha^2 + r^2)\,(C_1' \sinh b\alpha + C_2' \cosh b\alpha) + (\beta^2 - r^2) & \\
\cdot(C_3' \sin b\beta + C_4' \cos b\beta) &= 0 \,.
\end{aligned} \tag{A-23}$$

In order for nontrivial solutions to exist for the set of Equations (A-23), the determinant of the coefficients of Equations (A-23) must vanish. Solution of this frequency determinant leads to the following transcendental frequency equation:

$$2\,(1 - \cosh b\alpha \cos b\beta) + \frac{b}{(1 - b^2r^2s^2)^{1/2}}\left[b^2r^2\,(r^2 - s^2)^2 + (3r^2 - s^2)\right] \sinh b\alpha \sin b\beta = 0 \,. \tag{A-24}$$

Equation (A-24) is identical to that derived by Huang (reference 15) for this case. In order to determine the normal modal shape Y corresponding to a particular natural frequency, Equation (A-12) can be rewritten as follows:

$$Y/C_1 = \cosh b\alpha\epsilon + (C_2/C_1) \sinh b\alpha\epsilon + (C_3/C_1) \cos b\beta\epsilon + (C_4/C_1) \sin b\beta\epsilon \,. \tag{A-25}$$

Use of certain of the boundary conditions (A-23) in conjunction with relations (A-18) results in the following expressions:

$$C_2/C_1 = -\lambda\gamma \,, \quad \text{where} \quad \lambda \equiv \frac{\alpha}{\beta} \,, \quad \gamma \equiv \frac{\cosh b\alpha - \cos b\beta}{\lambda \sinh b\alpha - \zeta \sin b\beta} \,,$$

and

$$\zeta \equiv \frac{\beta^2 - s^2}{\alpha^2 + s^2}$$

$$C_3/C_1 = 1/\zeta$$

$$C_4/C_1 = -\gamma \ .$$

Substitution of these relations into Equation (A-25) gives the following result:

$$Y/C_1 = \cosh b\alpha\epsilon - \lambda\gamma \sinh b\alpha\epsilon + (1/\zeta) \cos b\beta\epsilon - \gamma \sin b\beta\epsilon \ . \quad \text{(A-26)}$$

It is noted that there are two errors in sign in Huang's Equation (53) which is otherwise identical to Equation (A-26) here.

UNCLASSIFIED

Security Classification

DOCUMENT CONTROL DATA - R&D

(Security classification of title, body of abstract and indexing annotation must be entered when the overall report is classified)

1 ORIGINATING ACTIVITY (Corporate author)

University of Oklahoma Research Institute

2a REPORT SECURITY CLASSIFICATION

Unclassified

2b GROUP

3 REPORT TITLE

DYNAMIC ELASTIC, DAMPING, AND FATIGUE CHARACTERISTICS OF FIBERGLASS-REINFORCED SANDWICH STRUCTURE

4 DESCRIPTIVE NOTES (Type of report and inclusive dates)

Final

5 AUTHOR(S) (Last name, first name, initial)

Nordby, Gene M., W. C. Crisman, and Charles W. Bert

6 REPORT DATE	7a TOTAL NO. OF PAGES	7b NO OF REFS
October 1965	81	50

8a CONTRACT OR GRANT NO.

DA-44-177-AMC-164(T)

b PROJECT NO.

c. Task 1P121401A14176

d.

9a ORIGINATOR'S REPORT NUMBER(S)

USAAVLABS Technical Report 65-60

9b OTHER REPORT NO(S) (Any other numbers that may be assigned this report)

10 AVAILABILITY/LIMITATION NOTICES

Qualified requesters may obtain copies of this report from DDC. This report has been furnished to the Department of Commerce for sale to the public.

11 SUPPLEMENTARY NOTES

12 SPONSORING MILITARY ACTIVITY

US Army Aviation Materiel Laboratories
Fort Eustis, Virginia

13 ABSTRACT

Research was conducted to determine the basic dynamic properties of fiberglass-reinforced plastic (FRP) sandwich structure suitable for use as a primary airframe structural material. The research program was carried out in two separate parts: (A) determining dynamic moduli and damping, and (B) determining fatigue behavior. In each part, two types of hexagonal-cell honeycomb core materials were investigated: 5052 aluminum foil and HRP (heat resistant phenolic) fiberglass. The selection of the sandwich configuration and fabrication procedures was based upon previous research carried out at the University of Oklahoma Research Institute for USAAVLABS (USATRECOM TR 64-37 and USAAML TR 65-66).

DD FORM 1 JAN 64 1473

UNCLASSIFIED

Security Classification

UNCLASSIFIED
Security Classification

14. KEY WORDS	LINK A		LINK B		LINK C	
	ROLE	WT	ROLE	WT	ROLE	WT
FRP Sandwich dynamic properties						

INSTRUCTIONS

1. **ORIGINATING ACTIVITY:** Enter the name and address of the contractor, subcontractor, grantee, Department of Defense activity or other organization *(corporate author)* issuing the report.

2a. **REPORT SECURITY CLASSIFICATION:** Enter the overall security classification of the report. Indicate whether "Restricted Data" is included. Marking is to be in accordance with appropriate security regulations.

2b. **GROUP:** Automatic downgrading is specified in DoD Directive 5200.10 and Armed Forces Industrial Manual. Enter the group number. Also, when applicable, show that optional markings have been used for Group 3 and Group 4 as authorized.

3. **REPORT TITLE:** Enter the complete report title in all capital letters. Titles in all cases should be unclassified. If a meaningful title cannot be selected without classification, show title classification in all capitals in parenthesis immediately following the title.

4. **DESCRIPTIVE NOTES:** If appropriate, enter the type of report, e.g., interim, progress, summary, annual, or final. Give the inclusive dates when a specific reporting period is covered.

5. **AUTHOR(S):** Enter the name(s) of author(s) as shown on or in the report. Enter last name, first name, middle initial. If military, show rank and branch of service. The name of the principal author is an absolute minimum requirement.

6. **REPORT DATE:** Enter the date of the report as day, month, year, or month, year. If more than one date appears on the report, use date of publication.

7a. **TOTAL NUMBER OF PAGES:** The total page count should follow normal pagination procedures, i.e., enter the number of pages containing information.

7b. **NUMBER OF REFERENCES:** Enter the total number of references cited in the report.

8a. **CONTRACT OR GRANT NUMBER:** If appropriate, enter the applicable number of the contract or grant under which the report was written.

8b, 8c, & 8d. **PROJECT NUMBER:** Enter the appropriate military department identification, such as project number, subproject number, system numbers, task number, etc.

9a. **ORIGINATOR'S REPORT NUMBER(S):** Enter the official report number by which the document will be identified and controlled by the originating activity. This number must be unique to this report.

9b. **OTHER REPORT NUMBER(S):** If the report has been assigned any other report numbers *(either by the originator or by the sponsor)*, also enter this number(s).

10. **AVAILABILITY/LIMITATION NOTICES:** Enter any limitations on further dissemination of the report, other than those imposed by security classification, using standard statements such as:

(1) "Qualified requesters may obtain copies of this report from DDC."

(2) "Foreign announcement and dissemination of this report by DDC is not authorized."

(3) "U. S. Government agencies may obtain copies of this report directly from DDC. Other qualified DDC users shall request through _____."

(4) "U. S. military agencies may obtain copies of this report directly from DDC. Other qualified users shall request through _____."

(5) "All distribution of this report is controlled. Qualified DDC users shall request through _____."

If the report has been furnished to the Office of Technical Services, Department of Commerce, for sale to the public, indicate this fact and enter the price, if known.

11. **SUPPLEMENTARY NOTES:** Use for additional explanatory notes.

12. **SPONSORING MILITARY ACTIVITY:** Enter the name of the departmental project office or laboratory sponsoring *(paying for)* the research and development. Include address.

13. **ABSTRACT:** Enter an abstract giving a brief and factual summary of the document indicative of the report, even though it may also appear elsewhere in the body of the technical report. If additional space is required, a continuation sheet shall be attached.

It is highly desirable that the abstract of classified reports be unclassified. Each paragraph of the abstract shall end with an indication of the military security classification of the information in the paragraph, represented as *(TS), (S), (C), or (U)*.

There is no limitation on the length of the abstract. However, the suggested length is from 150 to 225 words.

14. **KEY WORDS:** Key words are technically meaningful terms or short phrases that characterize a report and may be used as index entries for cataloging the report. Key words must be selected so that no security classification is required. Identifiers, such as equipment model designation, trade name, military project code name, geographic location, may be used as key words but will be followed by an indication of technical context. The assignment of links, rules, and weights is optional.

UNCLASSIFIED
Security Classification